UPPSALA
UNIVERSITET

Digital Comprehensive Summaries of Uppsala Dissertations from the Faculty of Science and Technology 1162

Sputtering and Characterization of Complex Multi-element Coatings

ERIK SÄRHAMMAR

ACTA
UNIVERSITATIS
UPSALIENSIS
UPPSALA
2014

ISSN 1651-6214
ISBN 978-91-554-8997-7
urn:nbn:se:uu:diva-229207

Dissertation presented at Uppsala University to be publicly examined in Polhemsalen, Ångströmslaboratoriet, Lägerhyddsvägen 1, Uppsala, Friday, 26 September 2014 at 09:00 for the degree of Doctor of Philosophy. The examination will be conducted in English. Faculty examiner: Dr. Gustaf Sjöblom (Senior Engineer, Surface Technology R&D, AB Sandvik Materials Technology).

Abstract
Särhammar, E. 2014. Sputtering and Characterization of Complex Multi-element Coatings. *Digital Comprehensive Summaries of Uppsala Dissertations from the Faculty of Science and Technology* 1162. 74 pp. Uppsala: Acta Universitatis Upsaliensis. ISBN 978-91-554-8997-7.

The thin film technology is of great importance in modern society and is a key technology in wide spread applications from electronics and solar cells to hard protective coatings on cutting tools and diffusion barriers on food packaging. This thesis deals with various aspects of thin film processing and the aim of this work is twofold; firstly, to obtain a fundamental understanding of the sputter deposition and the reactive sputter deposition processes, and secondly, to evaluate sputter deposition for specific material systems with low friction properties and to improve their performance.

From studies of the reactive sputtering process, two new methods of eliminating the problematic and undesirable hysteresis effect were found. In the first method it was demonstrated that an increased process pressure caused a reduction and, in some cases, even elimination of the hysteresis. In the second method it was shown that sufficiently high oxide content in the target will eliminate the hysteresis.

Further studies of non-reactive magnetron sputtering of multi-element targets at different pressures resulted in huge pressure dependent compositional gradients over the chamber due to different gas phase scattering of the elements. This effect has been qualitatively known for a long time but the results presented here now enable a quantitative estimation. For example, by taking gas phase scattering into consideration during sputtering from a WS_2 target it was possible to deposit WS_x films with a sulphur content going from sub-to-over-stoichiometric composition depending on the substrate position relative the target.

By alloying tungsten disulphide (WS_2) with carbon and titanium (W-S-C-Ti) its hardness was significantly increased due to the formation of a new titanium carbide phase (TiC_xS_y). The best sample increased its hardness to 18 GPa (compared to 4 GPa for the corresponding W-S-C coating) while still maintaining a low friction (μ=0.02) due to the formation of easily sheared WS_2 planes in the wear track.

Keywords: thin film, coating, magnetron sputtering, modelling, tribofilm, tungsten disulphide

Erik Särhammar, Department of Engineering Sciences, Solid State Electronics, Box 534, Uppsala University, SE-75121 Uppsala, Sweden.

ISSN 1651-6214
ISBN 978-91-554-8997-7
urn:nbn:se:uu:diva-229207 (http://urn.kb.se/resolve?urn=urn:nbn:se:uu:diva-229207)

Till min familj

List of Papers

This thesis is based on the following papers, which are referred to in the text by their Roman numerals.

I Sundberg, J., Nyberg, H., Särhammar, E., Gustavsson, F., Kubart, T., Nyberg, T., Jacobson, S., Jansson, U. (2013) Influence of Ti addition on the structure and properties of low-friction W-S-C coatings. *Surface and Coatings Technology*, 232(2013):340–348

II Nyberg, H., Sundberg, J., Särhammar, E., Gustavsson, F., Kubart, T., Nyberg, T., Jansson, U., Jacobson, S. (2013) Extreme friction reductions during initial running-in of W-S-C-Ti low-friction coatings. *Wear*, 302(1-2):987-997

III Sundberg, J., Nyberg, H., Särhammar, E., Kádas, K., Wang, L., Eriksson, O., Nyberg, T., Jacobson, S., Jansson, U. (2013) Tribochemically active Ti-C-S nanocomposite coatings. *Materials Research Letters*, 1(3):148-155

IV Särhammar, E., Strandberg, E., Martin, N., Nyberg, T. (2014) Sputter rate distribution and compositional variations in films sputtered from elemental and multi-element targets at different pressures. *International Journal of Materials Science and Applications*, 3(2):29-36

V Särhammar, E., Strandberg, E., Sundberg, J., Nyberg, H., Kubart, T., Jacobson, S., Jansson, U., Nyberg, T. (2014) Mechanisms for compositional variations of coatings sputtered from a WS_2 target. *Surface and Coatings Technology*, 252(2014):186–190

VI Särhammar, E., Strijckmans, K., Nyberg, T., Van Steenberge, S., Berg, S., Depla, D. (2013) A study of the process pressure influence in reactive sputtering aiming at hysteresis elimination. *Surface and Coatings Technology*, 232(2013):357–361

VII Berg, S., Särhammar, E., Nyberg, T. (2014) Upgrading the "Berg-model" for reactive sputtering processes. *Thin Solid Films*, 565:186-192

VIII Särhammar, E., Berg, S., Nyberg, T. (2014) Hysteresis-free high rate reactive sputtering of niobium oxide, tantalum oxide, and aluminium oxide. *Journal of Vacuum Science and Technology A*, 32(4):041517

Reprints were made with permission from the respective publishers.

Author's contribution to the papers

Paper I	Part of planning, all depositions of coatings, small part of analysis and evaluation, minor part of writing
Paper II	Part of planning, all depositions of coatings, small part of analysis and evaluation, minor part of writing
Paper III	Part of planning, all depositions of coatings, small part of analysis and evaluation, minor part of writing
Paper IV	Major part of planning, all depositions and analysis of coatings, part of discussions of the MC model, major part of writing
Paper V	Major part of planning, all depositions and analysis of coatings, part of discussions of the MC model, major part of writing
Paper VI	Significant part of planning, large part of the experimental work, significant part of evaluations and discussions, part of writing
Paper VII	Significant part of planning, all simulation work, significant part of discussions and evaluation, part of writing
Paper VIII	Major part of planning, all experimental work, analysis and evaluation, major part of writing

Related work

Särhammar, E., Nyberg, T., Berg, S. The influence of total processing pressure on the hysteresis behaviour in reactive sputtering. *IVC-18*, Beijing, August 23-27, 2010

Särhammar, E., Nyberg, T., Kubart, T., Berg, S. Hysteresis-free reactive high rate sputtering of vanadium oxide, tantalum oxide and niobium oxide from segmented metal/oxide targets. *ISSP 2011*, Kyoto, Japan, July 6-8, 2011

Strandberg, E., Särhammar, E., Nyberg, T. Estimations of energetic particle bombardment and compositional variations over films sputtered from compound targets by means of monte-carlo simulations. *RSD2011*, Linköping, Sweden, December 8-9, 2011.

Särhammar, E., Strandberg, E., Martin, N., Nyberg, T. Sputter deposition rate distribution versus processing pressure for light and heavy materials - experiments and simulations. *RSD2012*, Ghent, Belgium, December 13-14, 2012.

Särhammar, E., Strandberg, E., Nyberg, T. The influence of the processing pressure on the flux distributions of sputtered atoms from different materials and the induced compositional film gradients. *AEPSE 2013*, Jeju, Korea, August 25-30 2013.

Nyberg, H., Sundberg, J., Särhammar, E., Nyberg, T., Jansson, U., Jacobson, S. Performance and tribofilm formation of low friction W-S-N coatings. *In manuscript*

Contents

Abbreviations

CVD	Chemical Vapour Deposition
PVD	Physical Vapour Deposition
SRIM	Stopping and Range of Ions in Matter
SBE	Surface Binding Energy
DC	Direct Current
AC	Alternating Current
RF	Radio Frequency
MC	Monte-Carlo
DLC	Diamond-Like Carbon
TMD	Transition Metal Dichalcogenides
SEM	Secondary Electron Microscope
TEM	Transmission Electron Microscopy
RSD	Reactive Sputter Deposition

1. Introduction

Thin film technology is not only one of the newest sciences but also one of the oldest arts. The first thin films were purely decorative, painted on cave walls around 30000-40000 years ago. Another example comes from Egypt, more than 4000 years ago. Here gold was beaten into thin leafs (films) and put on statuaries for ornamentation and for protection purposes [1].

The modern thin film science was born in 1858 when J. Plücker noted the formation of a "beautiful metallic mirror" of platinum on the inside of a vacuum discharge tube [2]. Today, almost 160 years later, specific equipment in combination with extremely pure materials makes it possible to design thin films for various applications, manufactured with excellent control over its thickness ranging from a few atomic layers to several micrometres with an outstanding control over the film composition and structure. Thin films are now an essential part of everyday life, with wide-ranging applications across many fields stretching from microelectronics to automobile parts, and from windows on skyscrapers to the metallic coatings on the insides of bags of potato chips [3].

This technical field has undergone a rapid development the last four decades, where the microelectronic industry have been the driving force pushing the boundaries further and further, leading to expansions into new fields such as reflective/anti-reflective coatings, decorative coatings, semiconductor devices, diffusion barriers, sensors and wear-resistive coatings. Hence, today the thin film research is carried out on a broad front constantly evolving to be able to keep up with industrial as well as the societal demands of lower costs, better performance, less material consumption, smaller environmental impact and to help us take the next step into the future.

Thin films are deposited onto a bulk material (substrate) for two reasons; either the coating itself is the product (e.g. thin film solar cells) or it adds properties, which the bulk material alone could not achieve. For instance, by depositing titanium nitride (TiN) on a cutting tool made of steel, the lifespan is prolonged due to the properties of the coating; hardness, wear-resistant, and low friction. In addition to this, TiN thin films also exhibit a nice decorative golden colour. It is also possible to design and add more functionality to the thin film by, for instance, depositing several layers of different materials. An example of this is the optical interference filters, where layers of high and low refractive index are altered tens or hundreds of times. Another example is found in the integrated circuit industry, where multi-layered struc-

tures of semiconducting materials in combination with lithography patterning build the foundation of the integrated circuit industry with an endless variety of possible microstructures. Therefore, with knowledge of applied physics and material science together with all different material combinations and deposition techniques, the possibilities of making innovative and/or improved applications are virtually unlimited.

The source of the film-forming material may be a solid, liquid, or a gas, depending on deposition method used. There exist a number of different methods for thin film deposition [1, 4, 5]. The vast majority of these can be divided into three main groups; physical vapour deposition (PVD), chemical vapour deposition (CVD) and wet chemical processes. In a CVD and a PVD process, gases and solids respectively are used as sources. Both processes operate in a controlled atmosphere and have a high deposition rate, leading to less contamination of the thin film and a high throughput. Hence, the reason for their high industrial usage. In a CVD process, gaseous precursors are introduced into a reactor and a solid material is synthesized by chemical reactions. However, in order to get the reactive species needed for the synthesis of the solid, the gases have to be activated. This can be done in a variety of ways, e.g. by thermal activation, by applying an electric field or by electro-magnetic irradiation, etc. In a CVD process there exists a complex interplay between different reactions both in the vapour phase and at the vapour-solid interface. Further, an elevated substrate temperature is normally needed to facilitate high quality film growth. However, the necessary elevated substrate temperature puts high requirements on the substrate. In a PVD process, atoms (or molecules) are transferred from the source to the substrate where the growth takes place. This is done either by heating the source material to its melting point where after atoms are emitted from the source (evaporation) or by bombarding the source material with energetic ions causing ejection of atoms from the source (sputtering). Neither method needs elevated temperatures, which imply fewer requirements on the substrate, as compared to a CVD process. Another advantage with the PVD process is deposition uniformity as well as the possibility to scale up. Evaporation has a higher deposition rate than sputtering but the emitted atoms carry a lower kinetic energy [6]. The sputtered atoms, on the other hand, carry a relatively high kinetic energy making it possible to control the structure (from amorphous to large crystalline grains) of the growing film and hence the properties of the film. Today sputtering is the most frequently used deposition method for large area coatings (windows).

By adding several targets (sources) with different materials it is possible to deposit alloys. This is known as co-sputtering. The process is controlled by applying different powers to the targets, allowing the correct amount of respective target material to be ejected. Compounds (e.g. oxides and nitrides) can also be deposited by adding one or several reactive gases (oxygen, nitrogen, etc.) to the process. The reactive gas reacts with the target material and

forms a compound. This is known as reactive sputtering. By changing the reactive gas flow it is possible to control the composition of the film. However, the relationship between the film composition and the supply of reactive gas is very complex and highly non-linear and it usually involves hysteresis effects due to the complex interdependence between the different process parameters [7, 8]. Hence, it is of great importance to understand the process and to be able to control it.

By simulating the sputtering process as well as the reactive sputtering process, essential information can be obtained about the interdependency between the different processing parameters as well as their individual impact in the overall process. Therefore, simulations are an important and necessary tool in the search for control and optimization of the sputtering process, saving both time and money from extensive trial and error experiments as well as fundamental understanding of the sputtering process.

One aim of the present work is to obtain a fundamental understanding of the sputter deposition and the reactive sputter deposition processes through experiments and simulations. Another aim is to evaluate sputter deposition for specific material systems with low friction properties containing several elements, and to improve their properties and add new features. Special attention is given to the tungsten disulphide (WS_2) system, which has a layered structure and is known for its excellent low friction properties. However, in its pure form, WS_2 suffers from low hardness and low load-bearing capacity, which limits its use as a solid lubricant. Therefore, introduction of additional elements is needed to improve the mechanical properties, papers I-III. Intensive studies of the deposition process (papers IV and V), both experimentally and theoretically through Monte-Carlo simulations have been performed as well as characterization and tribological testing of the deposited thin films. Also, the reactive sputtering process is studied (papers VI and VIII) and simulated (paper VII) to optimize/stabilize the process through the elimination of the hysteresis effect.

This brief review of thin film science and technologies leads us to an introduction of the basics of the sputtering process in chapter 2, and further to simulations of the sputtering and reactive sputtering processes in chapter 3. Chapter 4 discusses the possibility of controlling the thin film growth to obtain specific structures and how to analysis the surface, bulk and properties of the deposited thin films. Chapter 5 gives an introduction to tribology and the possibility of designing smart protective thin films with versatile properties. In chapter 6, there is a discussion on the results and findings of papers I-VIII and chapter 7 gives a short summary of the results. The complete results are found in papers I-VIII at the end of this thesis.

2. Sputter deposition

Sputter deposition is a physical vapour deposition (PVD) process, well-established in the thin film industry. It gives high deposition rate, uniform thickness, reproducibility, quality and foremost is easy to scale up for large area depositions (several square meters big substrates). The process does not require elevated temperatures which enable the use of virtually any vacuum compatible substrate. This chapter gives a short description of the basic principles of physical sputtering and a somewhat more detailed discussion on Direct Current (DC) sputtering, Radio Frequency (RF) sputtering, magnetron sputtering and reactive sputtering.

2.1. Basics of the sputtering process

Physical sputtering is a process based on an incident energetic particle colliding with a solid (or liquid) surface (*Figure 1*) causing a sequence of collision events leading to ejection of material from the surface. The ejected atoms traverse the chamber until they condense onto the substrate or any other surface and form a film. The sputtering process is treated in a number of textbooks in great detail [1, 4, 9, 10].

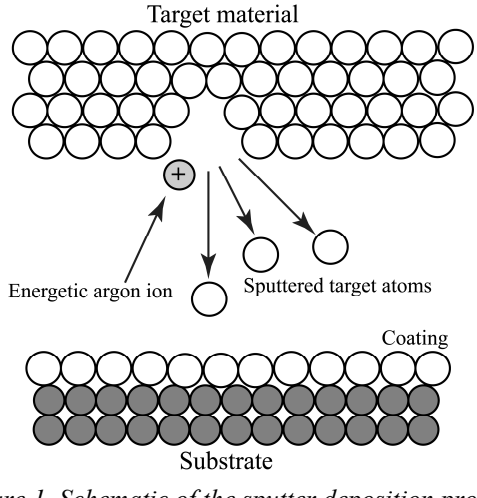

Figure 1. Schematic of the sputter deposition process.

Sputter deposition takes place in a closely sealed chamber evacuated by a vacuum pump (*Figure 2a*). A gas, usually argon, is introduced to the chamber and its supply is controlled by a mass flow controller. The processing pressure may be controlled by changing the supply of gas and/or by adjusting a valve between the chamber and the pump. The pressure is normally set in the range from around one to some tens of mTorr. The source material (target) is mounted to face the substrate, where the film grows. Positive argon ions in the plasma are accelerated towards the target, which upon impact cause a sequence of collisions in the target close to its surface (*Figure 2b*). Some atoms will recoil towards the surface and if their energy is greater than the surface binding energy (SBE), they will be ejected from the surface.

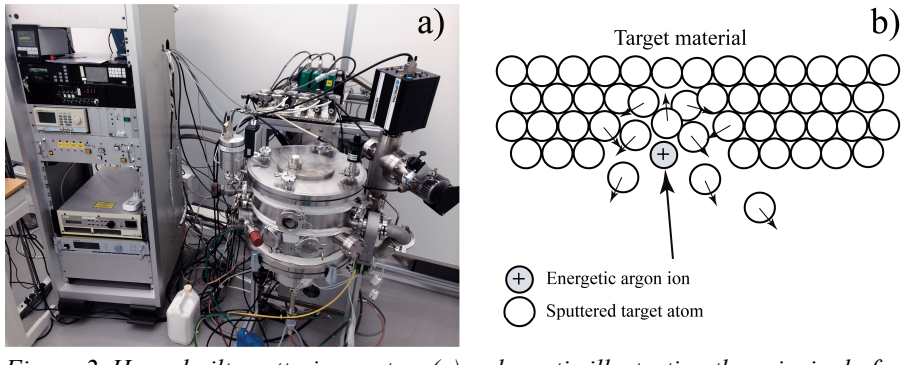

Figure 2. Home built sputtering system (a), schematic illustrating the principal of sputtering (b).

The number of sputtered species that are ejected by one incident particle is known as the sputtering yield. The sputtering yield is dependent on numerous parameters such as ion energy, angle of incidence, mass and atomic number of the ion and target material, crystalline structure, etc. For more precise estimation of the sputtering yield, as well as for a more complete description of the whole process, a number of advanced computer simulation programs have been developed in recent years, Stopping and Range of Ions in Matter (SRIM) [11], Transport of Ions in Matter (TRIM) [12], etc.

Generally, any energetic radiation composed of ions, neutrals, or clusters can cause sputter removal of material and emission of secondary electrons and photons as well as reflection of ions and neutrals. When energetic particles are bombarding the target surface, most of the particles energy is lost in the form of heat. Therefore external cooling is normally needed to prevent the target from melting. Only a small part of the incident energy (roughly half the SBE, see *Figure 3*) is carried away from the target as kinetic energy by the sputtered material [6].

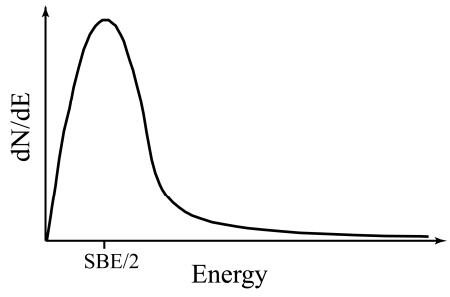

Figure 3. Energy distribution of sputtered atoms illustrating a peak close to half the surface binding energy (SBE).

For normal ion incidence the energy distribution exhibits a peak at half the SBE of the target material and tails off eventually as the inverse square of the energy, while the angular distribution of the sputtered flux normally follows a cosine law. The sputtered material traverses the chamber volume until it condenses onto the substrate and surrounding surfaces (chamber walls) to form a thin film of the target material. However, while traversing towards a surface, the sputtered species may encounter a number of collisions with gas particles depending on the gas pressure. In each and every one of these collisions some kinetic energy is lost and the direction is changed leading to a modification of the original angular and energy distributions of the sputtered flux.

2.2. Direct Current sputtering

The simplest form of Direct Current (DC) sputtering is the self-sustained DC glow discharge, first described by W. R. Grove in 1852 [13]. This is normally accomplished in an argon atmosphere by applying a potential between two electrodes, the negative cathode and the positive anode, see *Figure 4*. The target (cathode) is connected to the negative terminal of a DC power supply and the substrate, facing the target, can be either electrically grounded, biased or under floating potential.

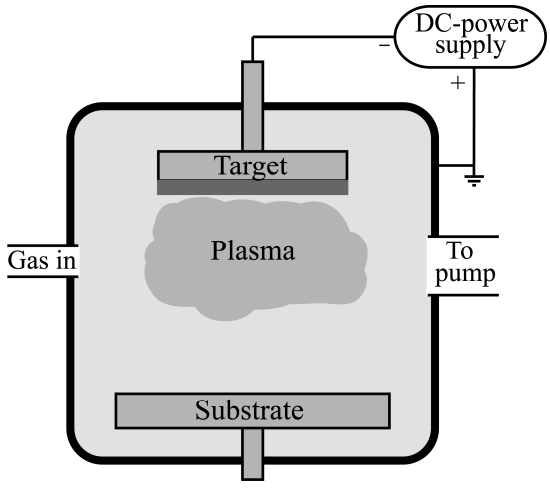

Figure 4. Schematic of a DC sputter system.

By applying a negative bias to the substrate, typically - 20 V to -200 V, a small fraction of the ions in the plasma will be attracted and accelerated towards the growing film. The ion bombardment will usually improve the quality of the film in terms of higher density, larger grain size and better crystallinity, etc.

To initiate and sustain a discharge in a diode or cathode sputtering system, a negative voltage in the range of 10^3 V is applied to the target. The argon gas pressure in the chamber is usually ranging from a few to 100 mTorr [1]. At low voltages there is no current running through the DC power supply, because there are so few free charge carriers (electrons, ions) in the system. The ones present have been ionized through cosmic radiation. As the voltage is increased, more and more energy is given to the charged particles. These particles will be accelerated towards either the target (ions) or the grounded chamber (electrons). As an electron traverses the chamber, it will constantly collide with argon atoms and lose energy. However, if the electron manages to travel a certain distance without colliding, its kinetic energy will be higher than the ionization energy the of argon atom. The electron then has a high probability to knock out an electron from the argon atom, creating a free-electron-free-ion pair. The new electron is affected in the same manner by the electric field as the old one and hence the chance of repeating the ionization event doubles and so on. However, for every newly created electron-ion pair, the distance to the anode is shortened. Finally, the distance is too short for the electrons to gain sufficient energy before they reach the anode and the generation of electrons and ions stops. In other words, the discharge dies out, since there are no more charged particles to carry the current. Fortunately, ions are also able to create free charged carriers. But because of their much larger collision cross-section, they have a small probability to gain sufficient energy to ionize an argon atom in a colli-

sion. However, when the ions collide with the target, there is a good chance that secondary electrons are emitted from the surface. The average number of electrons emitted per one incident ion is called the secondary electron coefficient (γ_{SE}). If one electron generates a sufficient number of ions as it traverses the chamber, so that this number multiplied by γ_{SE} is equal or greater than 1, the current or discharge will be self-sustained. Usually the voltage is increased until conditions for self-sustained discharge is reached. At this point, the current increase in an avalanche manner and the voltage decays until a balance is reached at typically around 1000 V. This equilibrium condition is known as a glow discharge.

Before the initiation of the discharge, the electric field between the cathode and anode is uniform. This is not the case after the discharge is started. The discharge consists of several regions where the two most important are called the plasma region and the cathode dark space region. The voltage distribution is shown in *Figure 5*. The plasma region is a bright glow caused by the excitation of the gas and the subsequent recombination followed by the emission of characteristic photons. The cathode dark space region corresponds to a sheath formed in front of the cathode (which is depleted from electrons giving less excitation and less emission).

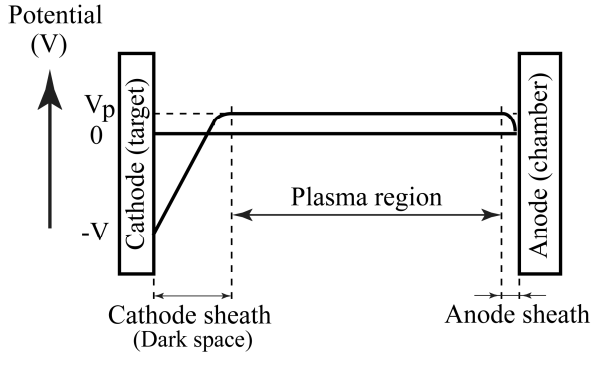

Figure 5. Potential distribution across a DC-glow discharge.

There is practically no electric field in the plasma region and the potential there, also called the plasma potential (V_p), is typically around 10 V. As a consequence of the differences in masses, and subsequently in mobility, between the electrons and the ions, the plasma potential is higher than that at the grounded anode. The electric fields in the system are typically restricted to the sheaths at each electrode (target and chamber). Ions that approaches the dark space sheath will be accelerated towards the target by this potential (the sum of the applied voltage (V) and the plasma potential (V_p)).

Since the target is the negative electrode in DC sputtering, any type of conducting material can be deposited. However, when using an insulating target the positive ions will be collected at the target surface until the total applied voltage is concentrated there. This will cause an extinction of the

discharge. For poorly conducting target materials it is possible to overcome this problem by using a pulsed DC voltage. This means that the DC voltage is applied in pulses (kHz range) so that the target surface may be neutralized between the pulses which prevent voltage build-up at the target. However, this approach cannot be used for insulating materials. Here an alternating target voltage (MHz range), a radio frequency (RF) needs to be applied.

2.3. Radio Frequency sputtering

RF sputtering has proven to be extremely useful for the deposition of insulators [1, 9]. The target is powered by an RF power supply, with a typical frequency ranging from 5 to 30 MHz (normally 13.56 MHz), while the chamber is grounded.

The AC signal causes the electrodes to alternately behave as cathodes and anodes. This makes electrons oscillate between the electrodes (inside the glow region) causing ionizing collisions with argon and because of that also reduce the need for secondary electrons to sustain the discharge. Electrons have a very high mobility which enables them to follow the periodic changes of the electric field. The much heavier ions on the other hand are hardly affected by the alternating field.

The sputtering system circuit can be thought of as two capacitors in series; one at the target and the other at the substrate and it has been shown that the area of the capacitor is inverse proportional to the voltage. Since the target electrode is much smaller than the total area of the grounded anode, a negative DC bias is generated at the target. Due to this negative target bias only a small part of the periodic cycle will be positive, see *Figure 6*. During this positive part of the cycle, only the much faster electrons will be able to arrive at the cathode and neutralize it before it becomes negative and starts to charge up again.

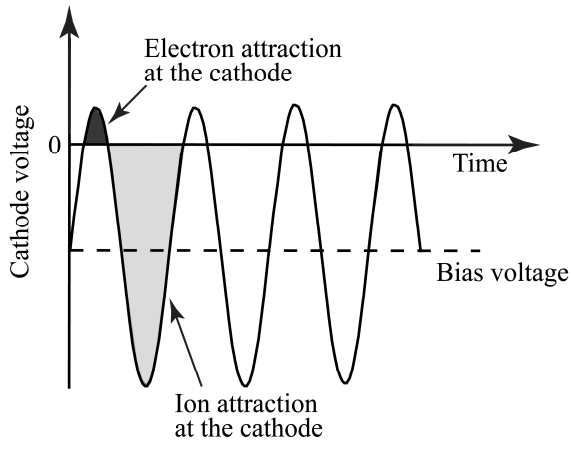

Figure 6. The cathode voltage as a function of time. Electrons neutralize the cathode during the positive part of the cycle.

RF can be used to sputter all target materials regardless of conductivity. However, as indicated in *Figure 6*, sputtering may only take place during the negative part of the cycle (when ions are attracted to the target). A consequence of this is a significantly decreased deposition rate compared to DC sputtering at the same power level. It is therefore impractical to use RF for sputtering of conductive materials.

2.4. Magnetron sputtering

A significant problem with a conventional diode or cathode sputtering system is its low ionization efficiency of its secondary electrons causing the need of a high process pressure and high target potential. The low generation of ions results in a low deposition rate which is even further reduced by losses to the surrounding surfaces (through gas phase scattering due to the high pressure). In magnetron sputtering this problem is solved to a large extent, by placing magnets behind the target, see *Figure 7* [1, 9]. The magnets introduce a strong parallel magnetic field close to the target surface, “trapping” the secondary electrons and hence making more efficient use of them. The electrons are forced to spiral around the magnetic field lines due to the Lorentz force, increasing the path length, which substantially increases the probability of ionizing collisions close to the target.

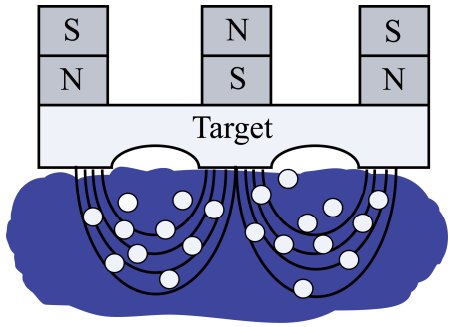

Figure 7. Illustration of the electron confinement in the vicinity of a magnetron. The magnetic field causes the electrons to move in spirals.

Thanks to the effective trapping of secondary electrons, the ionization efficiency is substantially increased. It is now possible to sustain a high density plasma (closer to the target) at lower gas pressures (in the range of a few mTorr) as well as lower target voltages (some few hundred volts). This results in higher deposition rates and a substantial reduction in kinetic energy of the energetic particles bombarding the growing film. The electron trap also reduces the electron bombardment of the substrate which makes it possible to coat temperature sensitive substrates.

A disadvantage with magnetron sputtering is usually the low target material utilization. The reason for this is the inhomogeneous erosion profile. Material is eroded much more efficiently where the magnetic field is strongest (parallel to the target surface, see *Figure 7*). As the erosion track, also known as a race track (*Figure 8*), becomes more pronounced, the sputtering rate drops due to the cosine distribution. However, by using rotating magnets or advanced magnetic field design, this material utilization problem can be circumvented.

Figure 8. Picture of a race-track formation on a circular Ti target.

2.5. Reactive sputtering

One of the most widely used techniques for deposition of thin films is reactive magnetron sputtering [8]. Especially in the field of large area coatings, where it is the leading technique.

In reactive sputtering, compound thin films are deposited by sputtering from metal, alloy or compound targets in the presence of a reactive gas. The reactive gas reacts with the sputtered material and forms a compound (e.g. an oxide when the reactive gas is oxygen). This makes it possible to deposit a wide variety of compounds (oxides, nitrides, carbides, sulphides, etc.) with a wide range of properties [14-17]. This versatility gives reactive sputtering a distinct advantage and is one of the reasons for its frequent use in industrial applications. *Figure 9* is an illustration of the reactive sputtering process. The reactive gas will form compound at all surfaces inside of the chamber where target material is deposited (substrate, chamber walls, etc.) or is present (at the target). When ions bombard the target surface, target and reactive gas atoms are the predominant ejected species from the surface.

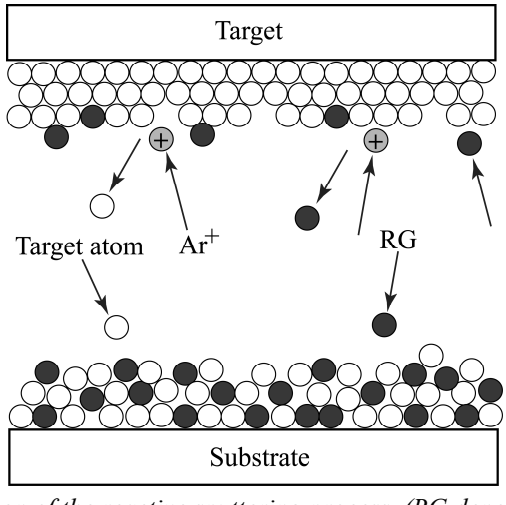

Figure 9. Illustration of the reactive sputtering process. (RG denotes reactive gas atoms and Ar^+ denotes positive argon ions).

Thin film properties are strongly dependent on the composition of the deposited film [14, 18]. Hence, there are great interests in being able to control the film composition. The most straightforward way is to adjust the reactive gas flow.

Simply put, a higher reactive gas flow to the system gives a higher concentration in the film. However, the relationship between the reactive gas flow and film composition is normally very non-linier and highly complex. When introducing a reactive gas like oxygen or nitrogen, the reactive gas atoms will react with the sputtered target atoms and form a compound film at

all surfaces in the chamber, including at the target surface. However, compound formation at the target (poisoning) normally causes the sputtering rate to drop, since compounds generally have a much lower sputtering yield than metals. This is due to the fact that the SBE is higher for compounds. The concentration of reactive gas in the film is normally quenched at a certain flow of gas. At this point P, see *Figure 10*, the reactive gas concentration corresponds to the stoichiometric composition of the compound. Increasing the reactive gas flow further will not change the composition but decrease the deposition rate. Since a reduction in deposition rate is highly undesirably, the optimum processing point is where the supply of reactive gas is precisely sufficient for obtaining stoichiometric films.

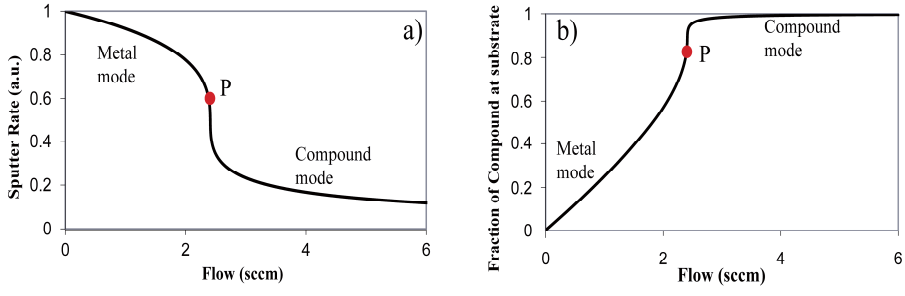

Figure 10. Simulations of the reactive sputtering process illustrating (a) the normalized erosion rate and (b) compound coverage of the substrate vs. reactive gas flow. To the right of the processing point P it is possible to deposit stoichiometric film composition.

Depending on the flow of reactive gas, one usually refers to two modes of operation, "metal mode" and "compound mode", see *Figure 10*. Metallic mode is characterized by a high deposition rate but the low reactive gas flow results in sub-stoichiometric predominantly metallic films. In compound mode it is possible to deposit stoichiometric films but with a considerably lower deposition rate. However, it is normally possible to deposit a stoichiometric composition with a high deposition rate in the region where the rate falls quickly versus the reactive gas flow (at around 2.4 sccm in *Figure 10*). However, the slightest increase of the reactive gas flow in this region, also known as the transition region, will cause a large shift in the processing conditions. *Figure 10* illustrates the non-linear behaviour of different processing parameters vs the reactive gas flow. Depending on materials system, the influence of the reactive gas flow may be of a very different nature. In fact, it is very common that the process shows hysteresis behaviour vs reactive gas flow.

2.5.1. Hysteresis

The effect of the hysteresis behaviour [7, 19] is seen in *Figure 11*, showing the erosion rate vs reactive gas flow. Here the transition region has expanded and it is no longer possible to deposit a stoichiometric film at position P, as it was in *Figure 10*. The solid line (between point A and C) inside of the transition region has now become an unstable/forbidden region for the process. By slightly increasing the reactive gas flow at point A, trying to reach point P, will cause an uncontrollable avalanche down to point B in compound mode. Hence the only way of depositing a stoichiometric film under these conditions is at a considerably much lower deposition rate down in compound mode. Further, it is not possible to just slightly decrease the reactive gas flow to get back to point A. Instead, the reactive gas flow has to be significantly decreased to a point C, where it will avalanche back up to D, in metal mode. The reactive gas flow can then be increased again to reach A. When the transition region behaves like this it is known as the hysteresis effect and is a significant problem in reactive sputtering.

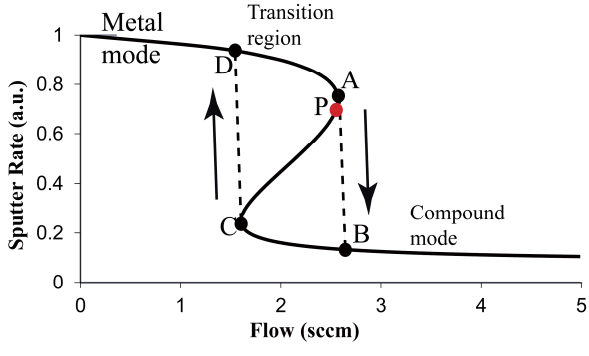

Figure 11. Simulation of the normalized erosion rate vs. reactive gas flow.

To understand the origin of the hysteresis effect observed in reactive sputtering we must consider the net consumption of the reactive gas. Reactive gas is consumed by the pump, the target, and receiving areas (chamber walls and substrate), denoted pump, target and receiving area respectively, see *Figure 12*. At steady state, the consumption rate of the reactive gas must equal the total gas flow supplied to the process.

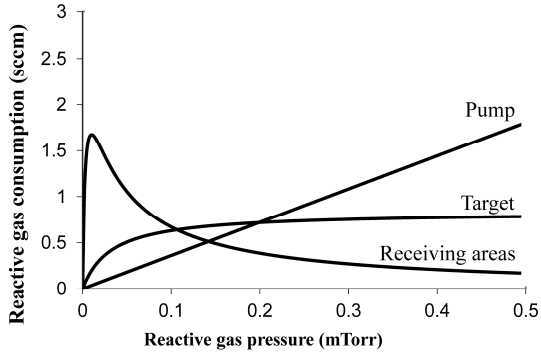

Figure 12. The three components of the reactive gas consumption as a function of the reactive gas pressure.

The consumption of reactive gas by the pump is linearly proportional to the pressure, see *Figure 12*. At the target the consumption of reactive gas must be equal to the number of out sputtered reactive gas atoms (at steady state). Since the target has a finite area the consumption must asymptotically approach a maximum value as the reactive gas pressure is increased, see *Figure 12*. This maximum value is reached when the target is fully covered by compound. However, it is the consumption of reactive gas by the receiving areas that is the cause of the hysteresis behaviour. This consumption depends on two factors, namely the available amount of reactive gas and the available number of unreacted metal atoms sputtered from the target. At low reactive gas pressures, the number of sputtered metal atoms is large while the available amount of reactive gas is small, resulting in a limitation of the consumption of reactive gas. As the reactive gas pressure (partial pressure) is increased, the target becomes more and more covered with compound resulting in less and less sputtering of metal atoms. Hence, the consumption of reactive gas is limited by the amount of unreacted metal atoms. Therefore, the consumption of reactive gas at the receiving areas starts from zero, passes through a maximum and goes down asymptotically to a value dictated by the total number of sputtered metal atoms from a fully compound covered target, see *Figure 12*. By adding the three consumption components and thereafter swapping the axis, yields the processing pressure versus the total consumption rate of the reactive gas. The latter, as noted above, must equal at steady state the total reactive gas inflow thus allowing interrelate the processing pressure and the total reactive gas inflow as illustrated in *Figure 13a*.

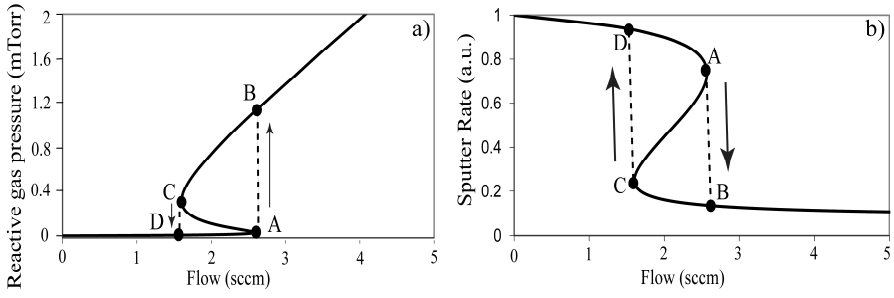

Figure 13. a) The partial pressure of the reactive gas and b) the normalized erosion rate vs the reactive gas flow.

To be noted in *Figure 13 a* and *b* is that both curves are multivalued in exactly the same specific region of the reactive gas flow and points A-D in *Figure 13a* correspond to A-D in *Figure 13b*. Hence, for the same reason as described about the process in figure 11 (erosion rate vs the reactive gas flow, the same as in *Figure 13b*), the process in *Figure 13a* will behave exactly the same. In other words, by varying the flow up and down, the process will follow the dotted lines in the direction of the arrows as shown in both *Figure 13a* and *b*. It should be noted that if the processing chamber is equipped with a unit capable of controlling the reactive gas partial pressure by adjusting the flow, the process can be made to follow the theoretical solid line between A and C, in *Figure 13* [20]. Unfortunately, this is a complex process for even a small laboratory system and therefore practically impossible for a large industrial system. However, by comparing *Figure 13b* with *Figure 10b* (both figures are showing the sputtering rate, except the latter has a hysteresis free process), it is possible to understand that the above hysteresis behaviour of the process is a consequence of the negative slope between A and C. Since *Figure 13 a* and *b* have the same hysteresis behaviour, the same is true for *Figure 13a* (showing the total consumption of reactive gas). With the help of *Figure 12*, it is possible to track the negative slope between A and C back to the consumption of gas at the receiving areas, since this is the only curve exhibiting a negative slope. Therefore, it may be possible to eliminate the hysteresis behaviour by manipulating the parameters controlling the three consumption components. This may be obtained by e.g. increasing the pumping speed (*S*) [21, 22] and thereby the slope of the corresponding curve, *Figure 14*. This causes an offset of the negative derivative and subsequently it is possible to obtain a ”total consumption vs. pressure-curve” without a negative derivative region and hence a hysteresis-free process.

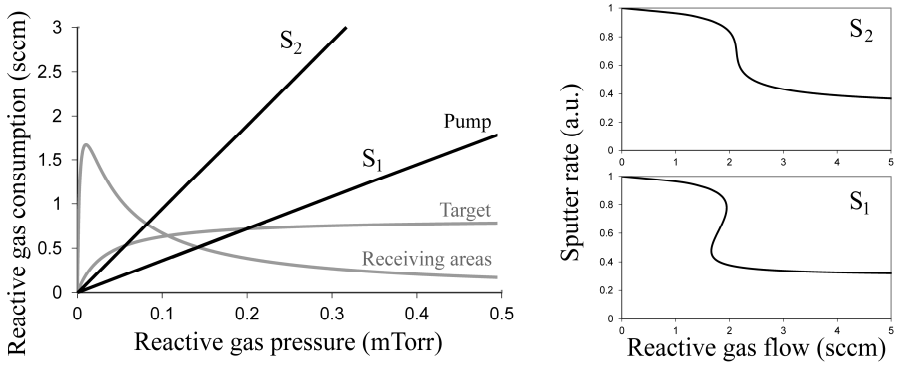

Figure 14. Simulations illustrating how the pumping speed affects the hysteresis behaviour in reactive sputtering. At the lower pumping speed (S_1) there is a pronounced hysteresis which is eliminated at the higher pumping speed (S_2).

However, "pumping" away the hysteresis is not realistic for large industrial vacuum systems. Other ways of eliminating the hysteresis is by using a small target area compared to the receiving areas [23], using a mixture of nitrogen and oxygen as a reactive gas [24, 25] or by using a sub-stoichiometric homogeneously mixed target [26] or a segmented target (paper VIII) both containing a certain amount of metal and oxide.

The reactive sputtering process is highly complex, depending on several different parameters such as, pumping speed, material reactivity, pressure, current, target size, etc. Hence, it is of great importance to understand the process and to be able to control it. By simulating the reactive sputtering process, essential information is given about how the process parameters are influencing the film growth.

3. Process modelling

In order to obtain fundamental understanding and to avoid expensive and time consuming trial-and-error development of the sputtering/reactive sputtering process, modelling is a valuable tool. By using simulations it is possible to predict the behaviour for different materials, reactive gases, processing conditions, etc. This chapter introduces a Monte-Carlo (MC) based simulation software, which can predict the sputter deposition rate distribution as well as the compositional variations over the chamber during sputtering from a multi-element target. Also, a simulation tool for the reactive sputtering process is discussed.

3.1.Monte-Carlo (MC) simulations of the sputter process

3.1.1. Introduction

Argon is normally used as the process gas in sputtering, responsible for the ejection of target atoms. A comparison between the physical size and mass of different elements (i.e. carbon with tantalum) makes it evident that they will behave differently when sputtered by argon. Think of a bike (carbon) colliding with a car (argon), compared to a car (argon) colliding with a bus (tantalum). This result in different scattering behaviour in the gas phase, see *Figure 15*.

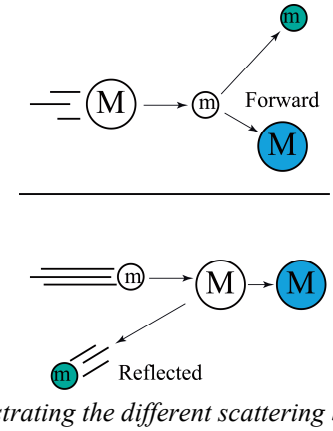

Figure 15. Schematic illustrating the different scattering behaviour of a heavy (top) and light (bottom) atom.

Therefore, when sputtering from a multi-element target the resulting film composition is almost always different from the target composition [27]. Hence, simulations are an important tool for fundamental understanding and to predict the behaviour for different elements in different processing conditions (pressure, target-to-substrate distance, processing gas, etc.) instead of time consuming trial and error testing.

3.1.2. Basic description of the MC-model

A simulation program was developed to gain a better understanding of the sputtering process. The MC based program is used to simulate more than $5x10^7$ individual particles, see *Figure 16*. Each particle is given an initial random position on an assumed race track on the target from which it is to be sputtered. Next SRIM is used to give the particle its initial direction (take-off angle) and energy. The program then follows each particle trajectory through the chamber and calculates its new position, direction and energy in every collision until it hits a surface, where it will stop.

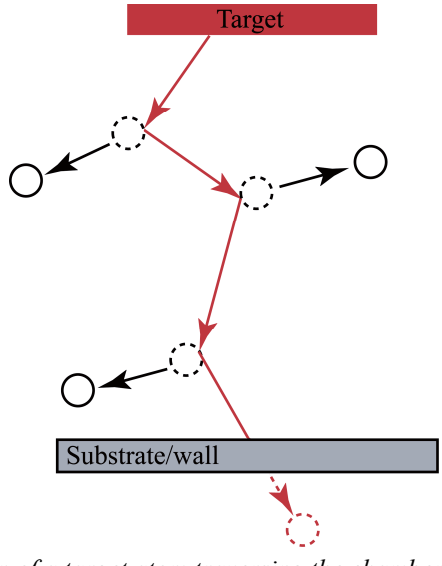

Figure 16. Illustration of a target atom traversing the chamber from the initial ejection at the target to the final condensation at the substrate/chamber wall.

When the particle collides with a sputtering gas atom/molecule, the interaction between the particles is determined by the hard sphere potential.

The dimensions and geometries of the chamber, as well as, target and substrate position are easily changed to match the actual vacuum chamber. All surfaces in the simulation chamber are divided into a multitude of mesh elements, see *Figure 17*.

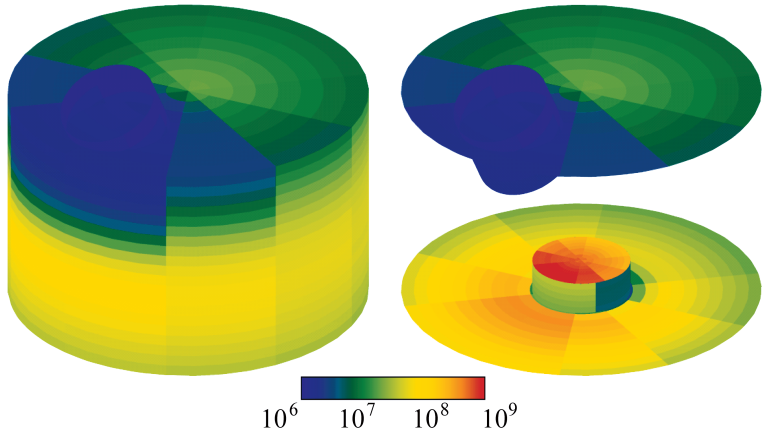

Figure 17. Illustration of the mesh elements and how the simulation results may be visualized. The colour bar follows a logarithmic scale.

Each mesh element registers all particles condensing upon it and the corresponding deposition flux is calculated. The latter is graphically represented using a colour bar legend for visualization purposes.

3.1.3. Results from the MC-model

MC simulations enable the possibility to see how different parameters affect the sputtering process. In paper IV and V, it is concluded that the major effect causing deposition rate variations as well as compositional variations over the chamber is the gas phase scattering (collisions between the sputtered atoms and argon). Depending on the pressure more or less collisions will occur before the atom is deposited. The number of collisions that the sputtered atom will undergo is dependent on the mean free path, which in turn is dependent on the size of the atom and on the argon pressure. In the collision with argon, the sputtered atom will be scattered (change direction) and lose energy according to the conservation of momentum rule. Here the difference in mass between the sputtered atom and the argon atom is important for the outcome of the collision. Small differences in mass will result in large energy transfers while large differences in mass will result in small energy transfers. Further, atoms lighter than argon will have a large scattering angle and can even be backscattered in a head on collision, while heavier atoms will proceed as before the collision and only experience small directional changes. *Figure 18* illustrates how the deposition rate varies over the chamber at low (0.27 Pa) and high (2.7 Pa) pressures for four elements with masses ranging from light (carbon) to heavy (tantalum). Argon is used as process gas. The purple lines indicate the trajectories of 40 randomly selected sputtered atoms for each simulation.

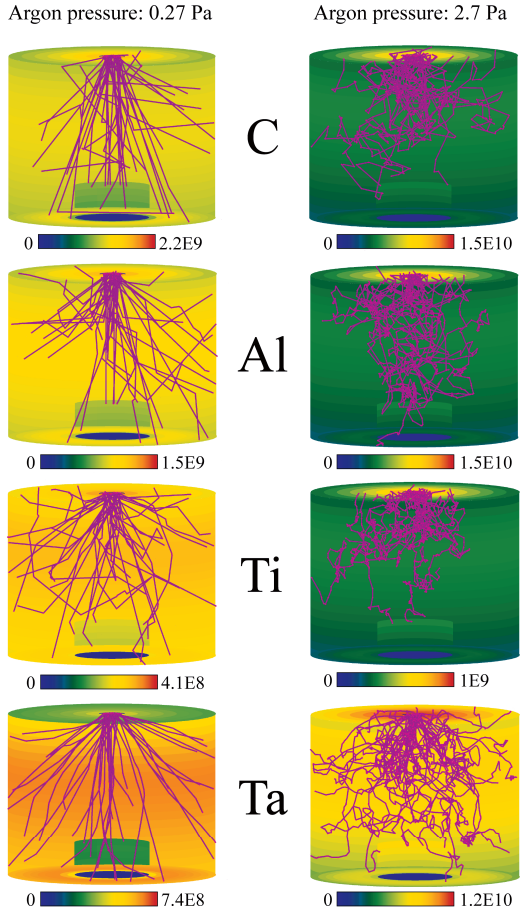

Figure 18. Simulations illustrating the different scattering behaviour as well as deposition rate profile for different elements at two different pressures.

As seen in *Figure 18*, the deposition rate distribution as well as the number of collisions before condensing at the substrate/chamber wall depends on the relation between the mean free path and the chamber dimensions. At low pressures the mean free path is large (few collisions). Therefore the simulated elements have no problems in reaching all surfaces inside of the chamber, except for tantalum that has to collide sufficient amount of times before it is backscattered and may reach the top surface of the chamber. However, due to the large mass of tantalum and the low number of collisions this event is very unlikely and is also illustrated in *Figure 18*, see colour bar.

At ten times higher pressure (2.7 Pa) the mean free path, being inversely proportional to the pressure, becomes ten times smaller for all materials. Here C, Al and Ti have difficulties reaching far out from the target surrounding areas and can be seen more as a diffusion process. Tantalum on the other

hand still maintains some original directionality but a large number of atoms are now being backscattered.

The large number of collisions causes the sputtered atoms to lose all or most of their kinetic energy resulting in a shift in their energy distribution towards much lower energies. *Figure 19* shows two simulations of titanium at 0.27 and 2.7 Pa respectively and the final energy distribution of the condensing atoms at the same three positions in both chambers.

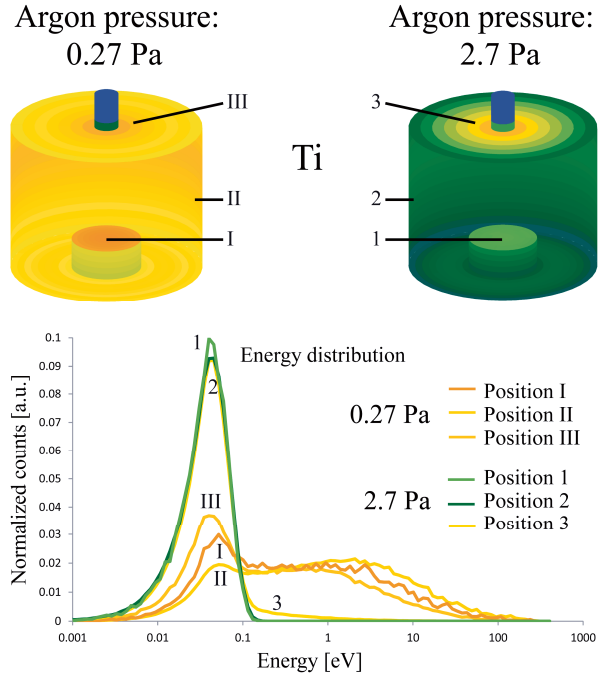

Figure 19. Simulations illustrating the energy distribution for sputtered titanium at three different positions at two different pressures.

At low pressures the three curves are slightly shifted from each other depending on position in the chamber (target-to-substrate distance and if the position is in line of sight). The target-to-substrate distance is of course important since a longer distance will increase the possibility of more collisions. However, position III is located just next to the target. But since the sputtered atoms needs to collide and be backscattered before they are able to reach this position they will also lose energy. With this in mind it is easy to understand why position II, at low pressure, has the highest average energy distribution (of position I-III), above 1 eV and the smallest amount of thermalized atoms (fractions of eV). Next is position I since it has a slightly longer target-to-substrate distance than position II. Last is position III, since all atoms needs to be backscattered to reach this position. At high pressure there are so many collisions that all atoms, regardless of position, will be

thermalized when deposited. A very small number of atoms reaching position 3 will have an energy slightly above thermalization.

3.2. Modelling of the reactive sputtering process

3.2.1. Introduction

The complexity of reactive sputtering makes process modelling an extremely valuable tool for studying and predicting its behaviour as well as developing new technical solutions. In 1987 Berg at al published a model explaining the gas consumption on various surfaces and the commonly occurring hysteresis effect [28, 29]. This model has been proven to agree well with numerous experimental observations reported in the scientific literature and is accepted worldwide [23, 24, 30].

The model is based on simple gas kinetics balance equations and can predict the composition of the deposited film, the partial pressure of the reactive gas, variations in the sputtering rate, the width and position of the hysteresis region, and the fraction of compound coverage of the target surface. Moreover, the model is very flexible and can easily be modified to account for reactive sputtering from an alloy or compound target, reactive sputtering using several reactive gases and reactive sputtering using several targets (co-sputtering) [31].

In the present work, the basic model (the Berg model) has been upgraded to account for several phenomena that have been limiting the original model. The upgraded version now sputters individual atoms instead of molecules, is dependent on the total pressure, and accounts for two implantation effects (direct ion implantation of ionized reactive gas atoms from the plasma and knock-in implantation of chemisorbed reactive gas atoms from the target surface) responsible for poisoning the sub-surface of the target (see paper VII). However, it is still a one-layer model and these modifications and additions do not make the mathematics more complicated or complex.

3.2.2. Upgrading the Berg model

Figure 20 illustrates the inside of a process chamber during the reactive sputtering process according to the mathematical outline of the upgraded Berg model. The process chamber consists of three parts that involves the reactive gas, namely, the target area (A_t), the collecting areas (A_c, the substrate and chamber walls) and the pump. The target and the collecting areas consists of two fractions each; pure metal ($1\text{-}\Theta_t$ and $1\text{-}\Theta_c$, respectively) and compound (Θ_t and Θ_c, respectively). The reactive gas can only form compound if it reacts with a free metal atom at the metal fraction. When this happens the metal is converted to compound and added to the compound

fraction. However, the reactive gas can also be direct implanted from the plasma (positive reactive gas atoms (RG^+)) and/or be knocked-in from the surface of the compound fraction into the sub-surface of the target. The implanted reactive gas atoms will react with metal atoms and form compound at the sub-surface of the target if they are implanted into the metallic fraction or diffuse out from the target and re-join the gas phase if they are implanted into the compound fraction.

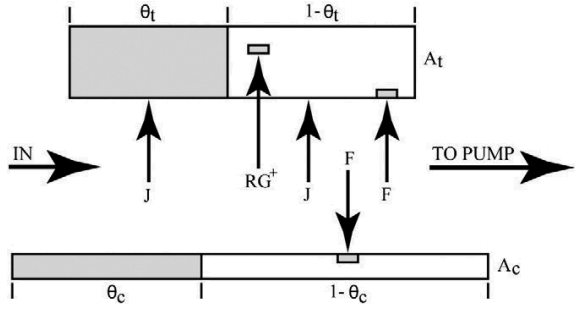

Figure 20. A schematic diagram of the inside of a process chamber corresponding to our mathematical outline of the reactive sputtering process, (paper VII).

Sputtering is assumed to take place over the entire target area, A_t. Moreover, when sputtering occurs from the compound part it is assumed that the compound molecule is split up into sputtered metal atoms (the reactive gas atom attached to the metal atom will be released back to the gas phase) and reactive gas atoms (the remaining metal atom will be added to the metal part of the target). The sputtered metal atoms are deposited over the entire receiving areas while the sputtered reactive gas atom may only condense if it arrives on the metal fraction of the receiving areas. When this occurs, the reactive gas atom is removed from the gas phase in a similar way as if it would be pumped out by the pump. From these assumptions it is possible to erect three basic balance equations describing the reactive sputtering process. A detailed description can be found in paper VII.

Target balance

At steady state, there must be an exact balance between the removal rate of reactive gas from compound and the compound formation rate by chemisorption and implantation. In other words, the reactive gas atoms going in must equal the reactive gas atoms going out. This defines the balance equation for the target.

$$\frac{J}{q}Y_k\theta_t^2 + \frac{J}{q}Y_c\theta_t = 2\alpha_t\frac{J}{q}F(1-\theta_t) + 2\alpha_i\frac{J}{q}\left(\frac{P}{P_A+P}\right)(1-\theta_t) \qquad (3.1)$$

where J is the total ion current density, q is the elementary charge, Y_k is the knock-in yield, θ_t is the compound fraction at the target, Y_c is the partial sputtering yield of reactive gas atoms, α_t is the reaction probability for a reactive gas molecule to form a metal compound, F is the flux of reactive gas molecules, α_i is the probability for a reactive gas ion to be implanted into the sub-surface, P is the partial pressure of reactive gas, and P_A is the partial pressure of argon.

The first term to the left represents the knock-in removal rate of reactive gas and the second term to the left represents sputtering of reactive gas. Together they represent the total removal of reactive gas from the target. The right hand side represents the total arrival rate of reactive gas to the target, where the first term is the poisoning contribution by chemisorption and the second term is the contribution of direct ion implantation. It is assumed that the ion-current carried by the reactive gas is proportional to the relative partial pressure of reactive gas. From equation 3.1, the fraction θ_t can easily be solved as a function of P.

Collecting areas

A similar balance equation can be defined for the substrate surface A_c, with one exception. At this surface there will be no sputter removal, only deposition and compound forming reactions by the reactive gas. We assume that all sputtered metal will be uniformly deposited at the collecting area A_c. However, there will only be a net contribution to 1- θ_c if the metal is deposited onto θ_c. Corresponding is true for the reactive gas. Hence, at steady state, there must be a balance between these two effects increasing and decreasing θ_c. This defines the balance equation for the collecting areas.

$$\frac{J}{q}\{Y_{mc}\theta_t + Y_{mm}(1-\theta_t)\}\frac{A_t}{A_c}\theta_c = 2\alpha_c F(1-\theta_c) \qquad (3.2)$$

Where Y_{mc} is the metal sputtering yield from the compound fraction, Y_{mm} is the metal sputtering yield from the metal fraction, θ_c is the compound fraction at the collecting area, α_c is the reaction probability for a reactive gas molecule to form a metal compound at the collecting area. The left hand side represents the total flux of sputtered metal atoms from the target being deposited at the compound fraction at the collecting area. The right hand side represents the compound formation at the colleting area by chemisorption. θ_c can easily be solved as a function of P, from equation 3.1 and 3.2.

Reactive gas

It should be understood from equation 3.1 that there will be no net consumption of reactive gas at the target, since the steady state balance states that what is going in must equal what is going out. Hence, there will only be two mechanisms consuming reactive gas supplied to the process chamber, name-

ly by forming compound at the colleting areas and by being removed by the system pump. This was not the case for the model used in section 2.5.1., where reactive gas was assumed to be consumed at the target. Neither model is wrong. They simply make different assumptions on how to account the reactive gas atoms forming compound at the target. Either way, in the upgraded model the two mechanisms consuming reactive gas define the balance equation for the reactive gas.

$$Q = 2\alpha_c F(1-\theta_c)A_c + PS \qquad (3.3)$$

Where Q (the left hand side) represents the total number of reactive gas atoms supplied to the chamber. The first term on the right side represents chemisorption at the collecting areas and the second term is reactive gas being pumped out of the system, where S is the pumping speed. Notice that the units for P and S must be selected to obtain atoms per unit time to fit the other terms in the equation.

4. Thin film growth, surface analysis and sample characterization

Thin film properties are strongly dependent on the structure and composition of the deposited film. A specific structure of the thin films can be obtained by controlling different process parameters such as the processing pressure, temperature, substrate bias, specific angle of incidence of the deposited atoms, etc. Further, a desired composition can be obtained by controlling the power fed to the different targets, processing pressure, reactive gas flow, target-to-substrate distance, etc. Hence, it is of great importance to know how these parameters affect the deposition process in order to optimize the properties of the resulting thin films. Surface analysis and characterization of the samples are vital in order to help perfect the process. This chapter gives a brief description of the film growth and techniques used for the surface analysis, characterization and testing of the deposited thin films used in this work.

4.1. Film growth

By controlling the process parameters during the sputtering process, it is possible to control the energy supplied to the growing film. By controlling the energy, it is possible to control the film growth and structure of the thin film and therefor its properties [32, 33]. The film growth can be divided into three stages; nucleation, island or layer-by-layer formation, and continuous film growth [1]. When an incident atom condenses/adsorbs (adatom) on the substrate, it will diffuse over the surface, searching for an energetically favourable position at the substrate where it can start the nucleation process. As the nucleus grows in two dimensions and reaches a critical size, either island or layer-by-layer formation will occur, depending on the film and substrate material. Island growth will take place if the most energetically favourable interaction is adatom-adatom, whereas layer-by-layer formation will occur if it is adatom-substrate. Beyond a critical layer thickness, the layer-by-layer formation will transform in to island growth. As the islands grow, they will subsequently coalescence and a continuous film will form.

As the continuous film grows, its microstructure evolution is highly dependent on the surface mobility of the adatoms. In general, an increased

adatom surface mobility will facilitate growth of larger crystals. Further, the adatom surface mobility is correlated to the amount of energy supplied to the growing film. This energy may be supplied as kinetic energy from the adatoms or as elevated substrate temperatures.

The kinetic energy is dependent on the number of collision the sputtered particles undergo before condensing at the growing film. At low pressures there are none or few collisions (depending on the mean free path and the target-to-substrate distance) in which the sputtered atoms will lose energy.

At high pressures, on the other hand, the sputtered atoms frequently collide with argon resulting in a shifted energy distribution to significantly lower energies (see *Figure 19*, section 3.1.3.).

However, as mentioned above in this section, the surface mobility of the adatoms can also be further enhanced by using elevated substrate temperatures. It is therefore possible to increase or decrease the substrate temperature and the process pressure, respectively, in order to increase or decrease the energy supplied to the film. However, some substrates are heat sensitive making it impossible to increase the temperature sufficiently for the formation of a certain structure. By using a substrate bias, a reduced temperature may be compensated for by ion bombardment. This may also sputter remove the most loosely bound atoms responsible for crystalline defects.

Another mechanism affecting the structure of the growth is the deposition rate [1]. If the deposition rate is low, sufficient time is given to the adatoms to diffuse to low energy positions. However, with a high deposition rate the adatoms are covered by new adatoms before they manage to find the best positions. E.g. high temperature and low deposition rate results generally in single crystals or large grained polycrystalline films, whereas a low temperature and a high deposition rate results in nanocrystalline or porous/amorphous films. Hence, proper control and understanding of the process parameters makes it possible to optimize the thin film structure and its properties.

Structure zone models are often used to illustrate how the processing pressure and substrate temperature influence the film structure [34-36]. *Figure 21* illustrates the Thornton diagram, which is divided into four zones, describing different types of structures and how they evolve depending on pressure and temperature (supply of energy). Zone 1 ($T_s/T_m<0.1$), is characterized by low substrate temperatures (T_s) in comparison to the melting temperature (T_m) of the film forming material, resulting in low mobility of the adatoms. Zone 1 has a porous structure consisting of thin columns composed of smaller more equiaxed grains and/or it may also be completely amorphous. At higher temperatures ($0.1<T_s/T_m<0.5$) the diameter of the grains increases and the intergrain voids begins to fill. Hence the structure passes in to a transition zone, zone T, with pronounced columnar structure. Here, surface diffusion is significant resulting in a competitive growth among neighbouring grains from which V-shaped columns of fast growing crystal planes

that will outgrow slowly growing crystal planes. At even higher temperatures $0.5<T_s/T_m<0.75$ (zone 2), bulk diffusion becomes possible causing migration of grain boundaries to minimize interface and surface energy [35]. Hence, the initial random oriented grains will be altered due to coalescence and grain coarsening and the resulting film structure will consist of large columnar grains. At very high temperatures $T_s/T_m>0.75$, zone 3, recrystallization may follow causing much larger in-plain grain sizes with an enhanced degree of texture.

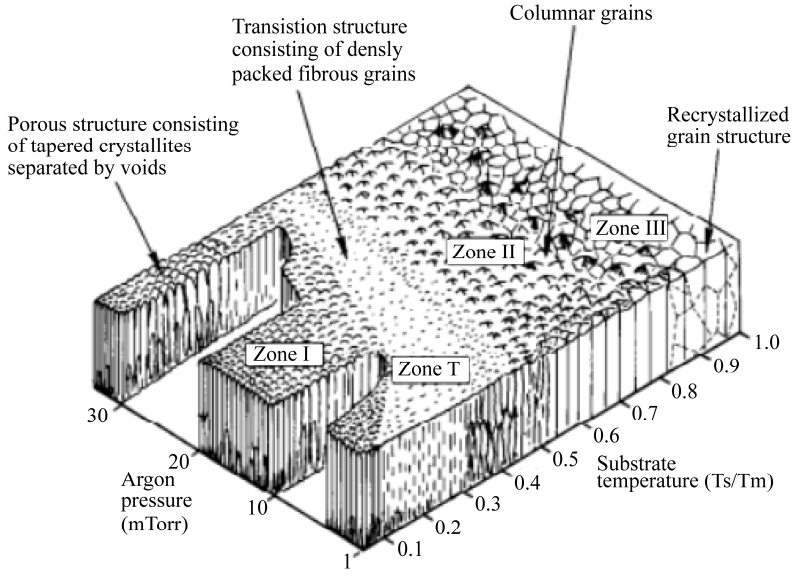

Figure 21. Thornton diagram illustrating the influence of processing pressure and substrate temperature on the microstructure of a sputtered single element metallic thin film [37].

The model described above is valid for a single metallic element. The addition of more elements (contaminants, dopants, or alloying elements) may strongly influence the film growth and structure, since different elements have different melting temperatures and hence the elements will be at different positions in the diagram for a specific substrate temperature [35]. E.g. element one in zone 2 while element two are in zone 1 or T. The additional element often segregates to surfaces and grain boundaries causing a reduction of the surface and grain boundary mobility of the first element. This results in limiting grain coarsening during coalescence causing a decrease in grain size and a reduction in preferred orientation. At higher concentrations of the added element, segregation causes encapsulation of the grains resulting in renucleation leading to a film structure containing grains with random orientations.

4.2. Surface analysis and characterization techniques

4.2.1. X-ray Photoelectron Spectroscopy (XPS)

XPS is a surface sensitive (normally <10 Å) technique by which elemental as well as chemical information of an atom can be extracted. This is done by bombardment of the sample by photons of sufficient energy to ionize an atom, and thereby causing ejection of a core electron from the surface. By measuring the energy of the ejected electron and knowing the energy of the photon it is possible to estimate the electron binding energy from the difference between these two quantities.

However, due to oxidation and contamination of carbon to the film surface, one normally sputters with an ion-gun into the bulk of the sample film for the characterization. Depending on material and energy of the sputtering ions, it will cause amorphization of the surface and may alter the composition of the sample through preferential sputtering. This method was used to analyse the composition of the coatings in papers I-IV and VIII.

4.2.2. Energy-Dispersive x-ray Spectroscopy (EDS)

By irradiating the sample with electrons, the atoms are ionized, causing the ejection of an inner shell electron leaving a vacancy in its former place. An outer shell electron fills in the vacancy and a photon with an energy equal to the potential energy difference between the two shells is emitted. The characteristic photon energy is unique for every element, so by measuring their energy it is possible to obtain elemental information of the studied material. From EDS it is possible to get information from a total depth of 1 μm.

This method gives mainly qualitative information but it is possible to also obtain quantitative information by making use of reference data. Qualitative information was extracted in papers I and II, while quantitative information was extracted in papers IV and V.

4.2.3. Electron Probe Micro Analyser (EPMA)

EPMA extracts the characteristic x-ray photons in the same way as in EDS. However, instead of measuring the energy of the x-rays, it measures their wavelengths. This increases the sensitivity, a better analysis of light elements, and a superior x-ray peak resolution (compared with EDS).

EPMA measurements was performed in Coimbra, Portugal, on a small number of samples, to help with the calibration of the sensitivity factors in EDS, used in papers I and II.

4.2.4. Raman Spectroscopy (RS)

In Raman spectroscopy, monochromatic light from a laser illuminates the sample. A small part of the photons will scatter inelastically with the sample molecules. The collision causes an energy exchange that results in either a higher or lower energy of the scattered photon compared with the incident photon. The difference in energy corresponds to a change in the vibrational and rotational energy of the molecule and gives information of its energy levels.

Raman spectroscopy was used in papers I and II.

4.2.5. Scanning Electron Microscopy (SEM)

In SEM, a beam of electrons is focused and scanned over a rectangular area of interest. Since electrons are charged particles, they can be accelerated. In SEM, electrons have a constant energy between 0.2-20 keV, which results in a wavelength smaller than the wavelength of visible light photons. Therefore, it is possible to get a larger magnification than in normal light microscopes, with magnifications up to some million times. As the electron beam collides with the sample surface, a number of interactions occur that can result in the emission of electrons or photons from the surface. A fraction of the emitted electrons is collected by detectors and the output is used to generate an image. This is possible since the position of the electron beam at the sample surface is synchronized with the corresponding location at the screen. Hence, the detectors know exactly where all detected electrons are coming from, disregarding of how many collisions they make on their way over there. By letting the number of emitted electrons detected from each point of the sample control the contrast of the corresponding point on the screen, it is possible to retrieve a detailed point-to-point image.

SEM was used in papers I-III to image the surface and cross section of the samples. The film thickness was also measured from the cross sections.

4.2.6. Transmission Electron Microscopy (TEM)

In TEM a focused high energy (100-400 keV) beam of electrons is transmitted through a very thin cross section of the sample. The electrons are interacting and scattered on their way through the sample. The transmitted scattered electrons are then focused into an image or diffraction pattern. Due to the electrons high energy, their wavelength is very small (much smaller than in SEM), making it possible to reach resolution down to the atomic level.

TEM was used in paper I-III to see the atomic configuration in the formed tribofilm.

4.2.7. X-Ray Diffraction (XRD)

In a XRD measurement, an incident beam of x-rays is interacting with the sample atoms causing the x-rays to diffract into different directions, which makes it possible to identify the atomic and molecular structure of the sample. By using different geometries it is possible to obtain information of all crystal planes in the sample. A θ-2θ scan (the angle of the incoming x-rays equals the angle of the outgoing x-rays), will only measure crystal planes that are parallel with the sample surface, while a glancing incident measurement (GI-XRD, the incoming x-rays are fixed with a small angle, 1-2 degrees, while the angle of the detector is varied) only measures planes perpendicular to the surface. The latter was used in papers I-III.

4.2.8. Profilometry

In a profilometer, a very light stylus is in physical contact with the sample surface. By slowly moving the stylus (or the sample) in one direction, the stylus is forced to follow the substrate surface topography. The small movements up and down are recorded and presented in the form of a graph. A step from the top of the coating down to the substrate can be obtained by drawing a line on the substrate with a water proof pen, prior to deposition, which later can be removed (together with the overlaying coating) with some alcohol. Film thickness was measured by means of this technique in papers I-V and VIII, either by measuring directly on the deposited samples or indirectly by measuring the film thickness of test depositions in order to obtain the deposition rate of that specific process.

4.2.9. White light interferometry

White light interferometry is an optical method used to measure the height variations/roughness of a sample surface and plot a 3-D profile. White light is illuminated on the sample where it will be reflected from different heights. This causes an interference pattern that can be transformed into a topographical image of the surface. Hence, it is possible to calculate the wear rate of the coatings by measuring the depth profiles of the scars obtained in the ball-on-disc measurement.

This was used in papers I and III, to calculate the wear rate of the coatings and balls.

4.2.10. Nanoindentation

In nanoindentation, a small diamond tip (Berkovich tip, with known geometry) is pressed into the coating. The small size of the diamond tip, allows shallow indentation depths (indentation depth compared to film thickness),

resulting in minimal influence from the underlying substrate. The force and depth of the indentation is continuously measured and makes it possible to calculate the hardness and Young's modulus of the coating.

Nanoindentation was used in paper I-III.

4.2.11. Spectrophotometry

A spectrophotometer measures the intensity of the reflection or transmission of a light as a function of wavelength. The principle is that a source lamp shines light into a monochromator, which diffracts the light into a rainbow of wavelengths in the range of 300-2500nm. Selected wavelength is then beamed at and transmitted through the sample. A photo detector behind the sample measures the intensity of the transmitted light and compares it with the transmission through the reference sample. The result is then plotted and viewed on a computer screen.

Spectrophotometry was used in paper VIII to measure the transmission of the samples.

4.3. Tribological testing

4.3.1. Scratch test

In a scratch test, a sharp tip is drawn over a selected area of the coating with constant speed and increasing load. At a certain critical load the coating will start to fail and crack. This measures the adhesive properties between the coating and the substrate and was used on all deposited coatings in papers I-III.

4.3.2. Ball-on-disc

In a ball-on-disc configuration, a ball is positioned at the tip of a fixed pin and put in contact with the sample with a predetermined constant normal load. The sample is attached on a disc, rotating with constant speed, making the ball slide in a small circle on the sample. The friction force is continuously measured during the test. By putting a sealed cover over the set up, it is possible to perform the test in different atmospheres (air, N2, Ar) with controlled/monitored humidity.

Wear between the ball and the coating causes a formation of a wear track on the coating, from which it is possible to calculate the wear rate with the help of white light interferometry, see 4.2.9.

Ball-on-disc was used on all deposited coatings in papers I-III. However, some of the coatings failed due to adhesion problems.

5. Tribology

This chapter gives a brief introduction to tribology and protective low friction coatings (solid lubricants). Also the possibilities to design smart multi-element coatings with several properties are discussed.

5.1. Introduction

Tribology is the science and engineering of interacting surfaces in relative motion and involves the study of friction, wear and lubrication. Tribology is part of everyday life through running, skiing, slowing down a car, or simply just by struggling to open a drawer. In a car engine, there are lots of moving parts in contact with each other, sliding up and down or back and forth. The friction between these interacting surfaces induces a higher energy consumption, resulting in a lower efficiency of the motor, since the friction will be converted into heat. As the surfaces are in sliding contact with each other, there will also be wear of the parts. Depending on the wear rate, the lifetime expectancy of the parts may be shortened (increased wear) or prolonged (decreased wear). However, wear is often an effect of friction and there are situations with low friction and high wear and the other way around. If the friction is increased, the heat will be increased, which in turn will cause an expansion of the metal parts, leading to even higher friction. This is what happens when a car engine seizes up. To prevent this from happening, a fluid lubricant is frequently used. The main purpose of the lubricant is to separate the surfaces and due to the separation reduce the wear and friction in the contact.

Today the demands of the mechanical systems are tougher than ever, with higher loads, longer duty cycles and rougher environments. At the same time environmentally hazardous additives, necessary for the performance of the lubricants, are banned due to stricter regulations of emissions. Moreover, in some situations it is not even possible to use lubricants. An example of this is the face seal located in pumps. Therefore, new mechanical systems, capable of working under extreme conditions are needed. Critical components in such systems are adhesive, protective, low friction coatings that may serve as solid lubricants. For instance, the number of pumps operated more or less continuously with pumping drinking water, waste water, etc. is enormous. The typical power loss in the seal (which cannot be lubricated) is up to 5

kW. By depositing a low friction coating, e.g. Diamond-Like Carbon (DLC) onto the seal, the friction may be reduced significantly, reducing the loss by approximately 1 kW per unit. If the seal is changed on 1250 units, 1250 kW will be saved, which is the equal of the production from four normally sized wind power plants (1500kW with around 20% output).

This is just one example of how much energy that can be saved by reducing the friction. Also a reduction in friction often results in a reduction in wear, which in turn would make the mechanical systems able to work harder/longer without the need for repair. Transferred to a global scale applied to transportation, industries, etc. the amount of saved energy and money would be enormous, not to forget the dramatic and positive environmental impact.

5.2. Tribological contact

5.2.1. Tribofilms

When two surfaces are in contact with each other, the local environment will be extreme with high temperatures and pressures. This puts high demands on the materials, which will change by deformation, transformation and chemical reactions. By depositing a thin film on one or both surfaces, the components will be protected against this local extreme environment. Thin films can be deposited in the range of a few nm to several µm thick, depending on its application/purpose. A tribological protective low friction coating is normally a few µm thick. If the coating is to thin, irregularities in the counter surface may break through, resulting in increased friction (metal-metal contact). If the thin film is too thick, the friction will be increased due to ploughing. With a tribological coating deposited on one of these surfaces, the top layer of the coating will change due to the harsh environment and form a layer providing low friction to the system. This top layer is what is known as a tribofilm and is between 5-50 nm thick, see *Figure 22*.

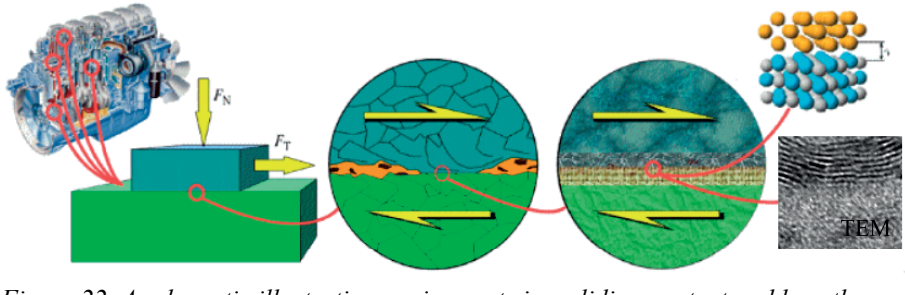

Figure 22. A schematic illustrating engine parts in a sliding contact and how the extreme local environment changes the top layer and forms a protective tribofilm (courtesy of Staffan Jacobson).

The formed tribofilm often contains more elements than the original coating due to contributions and reactions with the environment e.g. the counter surface, oxygen, etc. Hence, it is possible to design the original coating with elements that will use this contribution in the formation of the tribofilms. This is done in paper III. However, this is not always the case. Sometimes the tribofilm will be just a structured layer of the coating which is easier to shear. In these cases, it is possible to design the coating so that some elements form the tribofilm, which will contribute with low friction, while other elements are present in the bulk and forms a very hard protective layer on top of the component, see paper I-III. Therefore, it is possible to use softer, less wear resistant or simply cheaper materials for the coated component.

5.2.2. Solid lubricants

Two different families of low friction coatings are Diamond-Like Carbon (DLC) [38] and Transition Metal Dichalcogenides (TMD) [39]. DLC coatings consist of hard amorphous carbon and are today the most frequently used wear protective low friction coating used on components. However, there is a vital difference between DLCs and TMDs. DLCs are not an intrinsically triboactive coating, while TMDs are an intrinsically triboactive coating. A triboactive coating refers to a coating in a tribological contact that actively tries to form beneficial properties (low friction). However, DLCs may become triboactive with the help from surrounding atmospheres or oil additives, which in the same manner may remove the triboactive properties for TMDs. A problem for the DLC coatings is that the carbon structure will change into graphite if the temperature is too high. When this happens the friction and wear will increase and the coating will eventually fail. TMDs, on the other hand, have shown great results at elevated temperatures due to the removal of adsorbed water and will still provide low friction in temperatures, as high as 1000 °C in vacuum [40, 41]. DLC coatings will not be further discussed in this thesis.

TMDs are a large group of compounds with varying properties and crystallographic structures. However, the tribologically relevant materials with low friction properties have a layered hexagonal structure, but also a certain electronic structure is required to achieve the lowest possible shear resistance. These requirements limit the possible elements down to a small number with the general formula of MeX_2 (Me=Mo, W and X= S, Se, Te). These compounds have a highly anisotropic structure. Their low friction properties originate from their layered hexagonal structure, where a layer of transition metal atoms are sandwiched between two layers of chalcogen atoms, see *Figure 23* [42, 43].

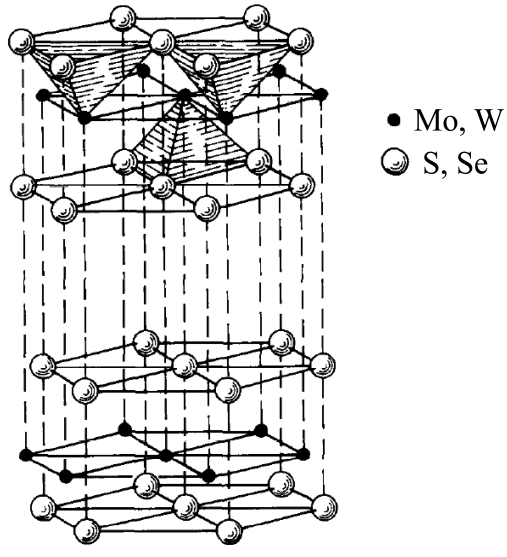

Figure 23. Crystal structure of MeX_2 (Me = Mo, W and X = S, Se) [42].

The bonds inside each "sandwich" are strong covalent bonds, while the bonds between two sandwiches are weak van der Waals forces. Further, the structure only contains unsaturated or dangling bonds at the edge of a plane or at defects. The electrons are preferentially located close to the metal atoms causing the negative charge to be contained within the layers, see *Figure 24*. This creates a net positive charge on the surface of the layers resulting in an electrostatic coulomb repulsion between the planes. Due to this, the sandwiches are easily sheared against each other, giving the material its excellent low friction properties [42].

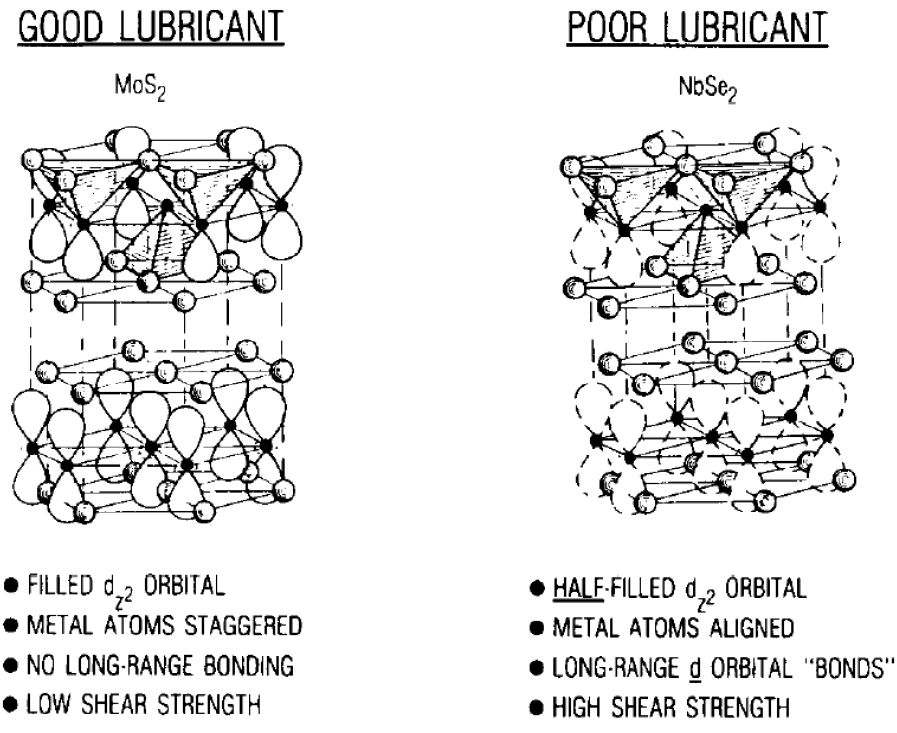

Figure 24. Illustration of the electronic structure of MoS_2 (good lubricant) and $NbSe_2$ (poor lubricant). MoS_2 has filled orbitals, while NbSe2 has half-filled orbitals which leads to a stronger bonding between the planes [42].

In a tribological contact (where one surface is coated with a TMD coating) the coating is initially worn and debris is transferred to and forms a film on the counter surface [44, 45]. During this initial process the top layer of the coating, as well as the transferred film on the counter surface, will be altered and the basal planes becomes oriented parallel to both surfaces, resulting in a very low shear resistance. Extremely low friction coefficients have been shown for MoS_2 ($\mu < 0.004$) [46] and slightly higher for WS_2, in vacuum with no contaminants present. However, in conditions when contaminants are present (humid air), the low friction properties will be heavily reduced. In humid air, water molecules will attack the dangling bonds at edge sites or at defects, causing the electronic structure to change from a repulsive to an attractive force between the layers, resulting in a higher shear resistance which causes a higher friction and wear [47, 48].

6. Results and discussion

This chapter is divided into three subsections; deposition of complex multi-element coatings for tribological applications, studies and modelling of the sputtering process at different processing conditions, and hysteresis elimination in reactive sputtering.

6.1. Deposition of complex multi-element tribological coatings

As mentioned in the previous chapter there is extreme local environments in the surfaces in a tribological contact, putting huge demands on the material used for the components. To protect the components, a hard, wear resistive, low friction coating can be deposited, which is able to endure the high pressure and load put on it. To obtain a coating with the various desired properties, one may mix several elements that individually do not possess all the required properties but collectively form a coating that meets the demands.

WS_2 is a well-known material with excellent low friction properties in dry and vacuum atmospheres. However, in its pure form, WS_2 is not suitable as a low friction coating due to its low hardness and low load-bearing capacity (the maximum pressure the coating may carry until it cracks). Further, it is sensitive to oxidation, which in a humid environment causes the formation of WO_3, resulting in less favourable tribological behaviour [48-50]. WS_2 can be magnetron sputter deposited in two ways; either by sputtering directly from a WS_2 target or by sputtering from a W target with the addition of S reactively through H_2S. The first alternative was used for the depositions of WS_2 in papers I, II, and V. Sulphur is a corrosive element with a high vapour pressure, meaning that sulphur deposited onto the chamber walls will be released during future depositions and contaminate the growing film (even if sulphur is not used). Due to this, a special (corrosive resistive) dedicated system is needed for depositions involving sulphur.

In papers I-III and V, such a sputtering chamber is used having the possibility to add sulphur reactively through H_2S (paper III). The system has three magnetrons in a sputter down position directed towards a rotating substrate table with the possibility to obtain substrate temperatures up to 500 °C.

As previously mentioned, deposited WS_2 in its pure form, is not suitable as a tribological coating. However, the addition of a third element, e.g. Ti [51], Cr [52], N [53], etc. may improve the mechanical properties of the material. The addition of a new element to a material system normally changes the microstructure and morphology of the coating [35, 51]. When going from a crystalline to an amorphous structure the hardness is typically seen to increase with one order of magnitude due to a reduction of easily sheared planes and decrease in coating porosity. The hardness may even be further increased if the added element, either by itself or with another present element, can form a hard phase. Promising results have been published for the W-S-C system where the coatings have become denser and harder while still showing low friction properties [54, 55]. In the W-S-C system, carbon forms an amorphous matrix which encapsulates nanocrystals of WS_2. Voevodin et al. explained the increased hardness to the formation of hard nanocrystals of tungsten carbide (WC), while the improved friction in humid atmospheres was a consequence of a "chameleon" behaviour where different atmospheres activated different elements in the coating. In dry atmospheres WS_2 provided low friction, while the carbon matrix was responsible for low friction in humid atmospheres [56]. However, Polcar et al. presented results indicating that WS_2 was responsible for the low friction seen in both dry and humid environments [57].

Even with the addition of carbon to the W-S-C system, the hardness is still rather low, since only a small part of the added carbon atoms bonds with tungsten to form WC while the remaining atoms stays free in the amorphous matrix. To further increase the hardness, a fourth element, Ti (which is a stronger carbide former than W) is added as well in papers I and II. The idea was that titanium carbide (TiC) would act as a hard protective coating while tungsten and sulphur would diffuse to the wear track and form easily sheared planes.

In paper I, four series were deposited, W-S-C RT and W-S-C-Ti RT at room temperature, and W-S-C HT and W-S-C-Ti HT at high temperature (300°C). Each series contained four samples with increasing carbon content from a few at% up to a maximum of 40 at% for the W-S-C series and 30 at% for the W-S-C-Ti series. It was found that the W-S-C coatings consisted of a crystalline phase of WS_x ($x<2$) in a matrix of amorphous carbon and amorphous WC. Increasing carbon contents lead to decreasing crystallinity for the WS_x phase and at high carbon contents x-ray amorphous coatings. The W-S-C-Ti coatings consisted of the same WS_x phase and matrix as the W-S-C coatings but with the addition of a titanium based carbide (TiC_xS_y) phase and that they were amorphous for low carbon contents. At higher carbon contents, the W-S-C-Ti coatings featured a columnar morphology and a crystalline carbide phase (TiC_xS_y).

Further, it is showed that the addition of titanium to the W-S-C system significantly increased the hardness of the material (W-S-C-Ti) in several

cases compared to W-S-C, see *Figure 25*. Further, Polcar et al have reported that the hardness for a W-S-C coating increases with increasing carbon contents up to 40 at%. Contents over this level causes the hardness to level out or even decrease [58]. A similar effect is seen in *Figure 25*. At low carbon contents the hardness is significantly increased from 4 GPa (W-S-C350 HT, where 350 indicates the carbon target power) to 18 GPa (W-S-C350-Ti HT) due to the formation of a titanium carbide phase (TiC_xS_y). At higher carbon contents, the W-S-C-Ti coatings still contains the titanium carbide phase but the coatings are more porous than their W-S-C counterparts resulting in only a small net effect of the measured hardness.

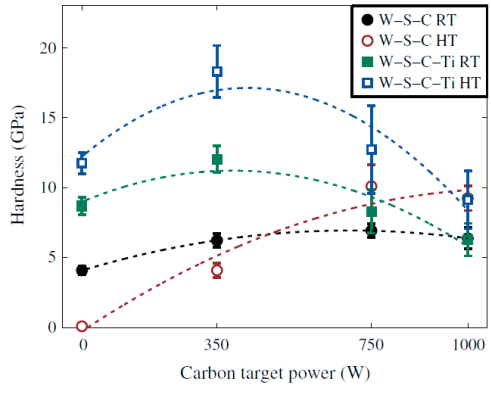

Figure 25. Hardness of W-S-C and W-S-C-Ti coatings as a function of the carbon target power used during sputter deposition. The lines are guides for the eyes, (paper I).

Ball-on-disc tests in a dry atmosphere showed that the friction was extremely high during the running-in phase for the W-S-C-Ti coatings. Later, during steady-state conditions, the friction level had dropped but in general to a higher level than what was seen for the W-S-C system. However, the best sample (W-S-C350-Ti HT) still managed to maintain the same low friction levels ($\mu = 0.02$) as the best W-S-C coatings. In a humid atmosphere there were no positive effects of the addition of titanium to the coatings. Both friction and wear rate were increased compared to the W-S-C system. However, the adhesion to the substrate might have been improved for coatings containing titanium compared to W-S-C coatings, independent of atmosphere.

Analysis of the coatings, as-deposited and after ball-on-disc test reveals the formation of a crystalline tribofilm with aligned WS_2 planes in the wear track of the W-S-C-Ti coatings, see *Figure 26*. This could seem strange since most coatings were x-ray amorphous and therefore had an absence of crystalline WS_2 in their coatings. However, Gustavsson et al. has recently shown that only PPM levels of an element is needed for the formation of a beneficial tribofilm in the sliding contact [59]. Therefore, the experiments

confirmed our initial assumptions since we managed to significantly increase the hardness of the material while in the same time easily sheared WS_2 planes were created on top of the coating in the contact between the surfaces.

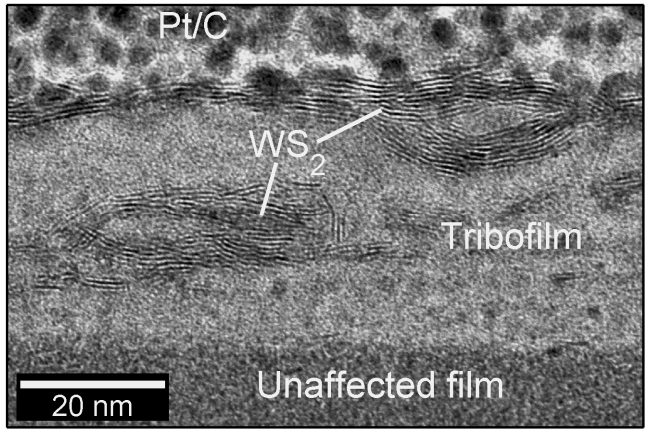

Figure 26. TEM cross-section perpendicular to the sliding direction from the wear track of a W–S–C350–Ti HT coating. Horizontally aligned WS_2 planes have formed on the top surface, as well as within the amorphous tribofilms, (paper I).

One thing noticed during the ball-on-disc test was the difference in initial friction (running-in time until steady state) between the W-S-C and W-S-C-Ti systems, which were extremely high for the latter system, see *Figure 27*. The mechanisms behind this running-in behaviour are further investigated in paper II, from studies of the wear tracks at an early stage as well as later at steady-state friction conditions. Analysis of the initial wear tracks in the W-S-C-Ti system shows almost exclusively the presence of TiO_2, compared to almost immediate formation of WS_2 in the W-S-C system. The TiO_2 is believed to originate from the native oxide of the coating. At steady state, the friction has gone down, due to the removal of the oxide layer which makes it possible for the formation of WS_2. There is, however, still some TiO_2 in the wear tracks.

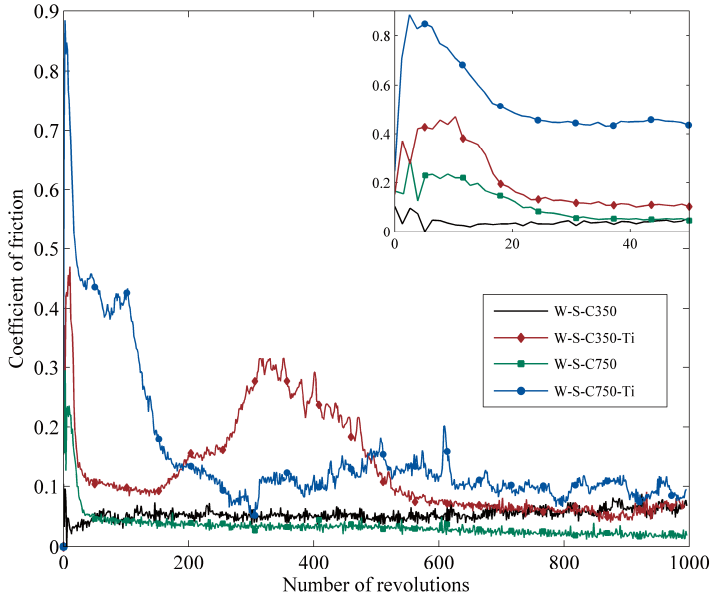

Figure 27. Coefficient of friction of the coatings from the first 1000 revolutions in ball-on-disc tests. The inset gives a detailed view of the first 50 revolutions, (paper II).

In paper III, the new TiC_xS_y phase is further investigated. Here sulphur is added reactively through H_2S while titanium and carbon are deposited by pulsed DC magnetron sputtering from a Ti-target and a C-target. By increasing the reactive gas flow of H_2S the sulphur content in the coatings goes from zero up to 21 at%. Further analysis shows that sulphur is incorporated into the TiC cell (by replacing C) and that the cell parameter is increasing for higher sulphur contents. The coating with highest sulphur content had a cell parameter of 4.81 Å, which is more than a 10% increase compared to pure TiC. Theoretical calculations based on supercells containing 64 atoms confirm that sulphur is indeed dissolved into the TiC cell forming a new TiC_xS_y phase and that the cell parameter increases in accordance with the deposited coatings.

Annealing tests were performed for 60 minutes in vacuum at 500 °C. After annealing, analysis showed lower sulphur content in the coatings and that the cell parameter had decreased in size. This implies that sulphur may be released from the TiC_xS_y phase.

Ball-on-disc test against steel balls showed that the friction is somewhat reduced (although still high friction levels) for higher sulphur contents in the coating. This could be due to that an increased sulphur content causes a decrease in grain size of the TiC crystals (see section 4.1.), as well as to a less pronounced texture of the coatings, which is expected to increase the cohesion and toughness of the coatings. Another explanation could be the for-

mation of FeS (Fe from the steel ball) which is a known solid lubricant, just not a low friction one. However, by switching out the steel ball to a tungsten coated ball, the friction was significantly decreased, see Figure 28. TEM analysis of the wear track and counter surface showed the formation of a tribofilm with aligned WS_2 planes. It is therefore demonstrated that sulphur can be released from the TiC_xS_y phase by activation from a counter surface.

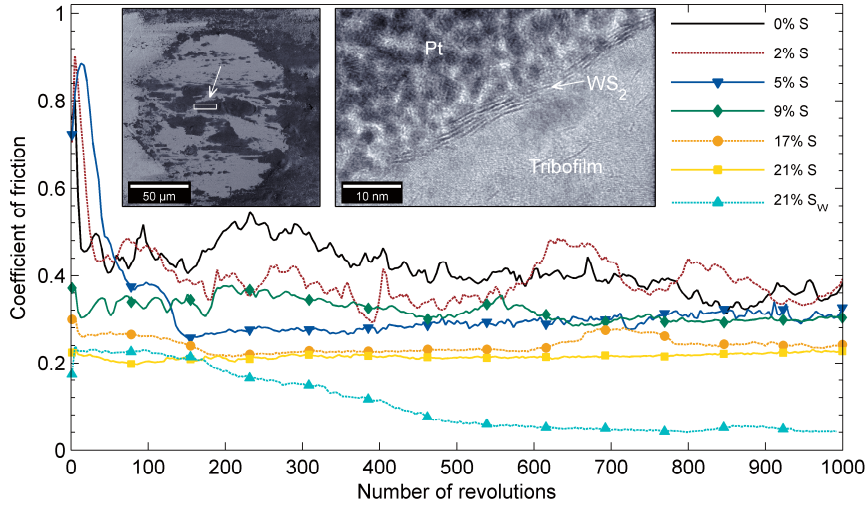

Figure 28. Coefficient of friction of all deposited coatings running against steel balls. Also, the coating with the highest sulphur content was tested against a tungsten-coated ball (indicated by a subscript W). The inset is an SEM micrograph of the wear scar on the W-coated ball, where the dark patches are the tribofilm and the bright areas is the W coating, and a TEM cross-section prepared from the marked area in the tribofilm. The bright area to the lower right corresponds to the mostly amorphous tribofilm, while the dark and bright stripes are a few atomic layers of tribochemically formed WS_2, aligned with the easily sheared planes along the sliding direction, (paper III).

A significant problem for tribological coatings is adhesion to the substrate. Several coatings in papers I-III were not possible to evaluate tribologically due to poor adhesion of the coatings during ball-on-disc tests. Most coatings that failed at early stages of testing showed reasonably low initial friction, which later could have shown to perform excellent. Therefore, the results presented in papers I-III are mainly based on coatings that exhibited sufficient adhesion, and thus could be evaluated and compared.

To improve the adhesion, the substrate surface is pre etched by ions bombarding the surface and thereby removing impurities, just before the deposition of the coating. Also, a thin interlayer of titanium, roughly 60 nm thick, can be deposited just before the deposition of the coating [53]. However, the

impact of this interlayer is hard to evaluate since some coatings did stick before the introduction of the interlayer and some coating still failed after the introduction of the interlayer. Either way, the titanium interlayer will not deteriorate the adhesion of the coating.

Other ways of improving the adhesion for TMD coatings are to control the process parameters during the microstructure growth (see section 4.1.). When depositing TMDs, it is possible to either deposit the material with its basal planes perpendicular to the surface (type I), with its basal planes parallel to the surface (type II), or as an amorphous coating [43, 60, 61]. The type II structure reduces the running-in time, since the basal planes already are parallel to the surface. However, this often leads to high concentrations of defects and poor adhesion since the basal planes are relative inert. Type I, forms a columnar structure with its highly reactive edge sites exposed. This causes poor tribological properties since the columns rather detaches than reorients at the surface, but better adhesion may be achieved to the substrate. For the amorphous coatings varying results have been shown [62]. The addition of new elements to the TMD coating causes the microstructure to change into a nanocrystalline or amorphous structure which is denser and in many cases shows stronger adhesion. This was noticed in papers I and II, where the addition of titanium to the W-S-C system seemed to have better adhesion than the W-S-C coatings. Further, a number of experiments using substrate bias were carried out to investigate if the adhesion could be improved. However, in those experiments we only observed a denser coating. Either way, good adhesion is a very important factor for tribological coatings and more research is needed in this area.

6.2. Studies and modelling of the sputtering process at different processing conditions

It was observed, in papers I and II, that sputtering from a WS_2 target resulted in sulphur deficient films. It is generally accepted that slightly sub-stoichiometric films are commonly observed when sputtering from a compound target [27]. For instance, when sputtering from oxide targets small amounts of oxygen must be added to ensure a stoichiometric composition. However, in papers I and II, the S/W ratio was close to one (WS) instead of two (WS_2), which corresponds to the composition of the sputtered material. In the literature, this is explained purely by re-sputtering of the film due to energetic particle bombardment (negative ions, reflected argon and high energy neutrals) of the substrate [63, 64]. Further investigations of sputtering from a WS_2 target showed a variation in film compositions depending on the substrate position relative to the target. The observed sub-stoichiometry could not only be explained by energetic particle bombardment, implying

that several additional effects such as differences in initial take-off angles, sticking coefficients and gas phase scattering could also be responsible for the observed sulphur deficiency [27, 65-67].

To explore potential mechanisms responsible for the observed compositional variations, further investigations were performed on a much simpler system consisting of two metals (paper IV). Here the difference in sticking coefficients and re-sputtering effects are insignificant. To gain even further information, a Monte-Carlo based simulation tool was developed (described in section 3.1.) where each particle is followed from the target to the chamber wall/substrate. This gives deposition profiles for the different elements and makes it possible to predict the film stoichiometry. The results revealed significant pressure dependent compositional variations over the chamber. Comparison with experimental results showed adequate agreement and it was concluded that such variations are due to the different nature of the scattering in the gas phase which is predominantly dependent on the mass and size of the atoms.

The main conclusion of paper IV is that the different scattering behaviour for different elements may cause significant pressure dependent compositional gradients over the chamber. This is qualitatively well known since long time. However, since it investigates material combinations ranging from light (carbon) to heavy (tantalum) over a large pressure interval where sputtering normally occurs, it may be used as a guideline when sputtering from multi-element targets. The results can be extrapolated and thereby predict deposition profiles and compositional gradients for arbitrary materials combinations and processing pressures.

The simpler two-metal systems, in paper IV, confirmed the validity of the Monte-Carlo based simulation tool. In paper V, a more complex material system (WS_2) is investigated. Here, sputtering from a WS_2 target was studied in more detail and it was concluded that the previous explanations for the sulphur deficiency in sputtered films was not sufficient to explain the compositional variations. It was concluded that in addition to re-sputtering of the film due to energetic particle bombardment, one must also take scattering in the gas phase into account. In fact, the latter effect was demonstrated to be significantly larger than the previous one. By moving the substrate to an off axis position closer to the target, energetic particle bombardment of the substrate is suppressed, see *Figure 29*. As seen in section 3.1.3., sulphur will scatter more than tungsten due to its much smaller mass. As a result more sulphur will reach the off axis location than tungsten. Analysis of the off axis samples showed an over-stoichiometry with the maximum of $WS_{5.5}$ measured at the position closest to the target.

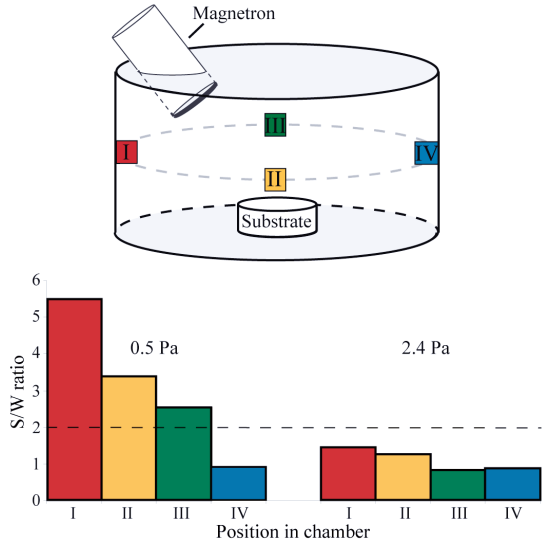

Figure 29. Schematic of the experimental chamber illustrating the position of the substrates during off-axis deposition. The graph illustrates experimental compositions of tungsten sulphide films deposited at these positions (I-IV) at two different pressures (0.5 and 2.4 Pa). The dashed line in the graph represents the target composition (WS_2), (paper V).

Donnet et al. reported that the low friction properties of MoS_2 were strongly connected to the stoichiometry of the coating [68]. Since the systems (MoS_2 and WS_2) exhibit significant similarities, it was assumed that the same was true for the WS_2 system. However, Gustavsson et al. showed that sulphur contents in the PPM level is sufficient for the formation of easily sheared WS_2 planes due to sulphur and tungsten strong diffusion tendency and its affinity to form WS_2 in the wear track [59]. Therefore, as concluded in papers I and II, the sulphur deficiencies observed is not a problem for the tribological coatings. However, WS_2 can be used in other applications, e.g., solar cells where stoichiometric composition is of great importance.

It should be pointed out that in these off axis deposition, no morphological or structural analysis was performed, only film composition measurements. However, a stoichiometric or over-stoichiometric film with a specific structure may be deposited by adding energy through elevated substrate temperatures and/or the use of substrate bias. Further, the samples were stationary during the deposition, resulting in an inhomogeneous film thickness. Normally this is solved by using a rotating substrate table.

6.3. Hysteresis elimination in reactive sputtering

It has previously been shown that the processing pressure is important for the sputtering process (papers IV and V). For instance, elevated pressures reduces the kinetic energy of the sputtered atoms, which may result in less favourable growth conditions and it causes more scattering in the gas phase which results in compositional variations over the chamber. However, in the literature there were no reports of how such a basic parameter, as an elevated pressure, would affect the reactive sputtering process, especially the hysteresis behaviour.

In paper VI, this was further studied for four different reactive gas/material systems (Al, Mg, Y in Ar/O_2 and Ti in Ar/N_2) with high and low reactivity to emphasize the influence from the increased processing pressure. These materials were chosen because they are self-limiting to a stoichiometric composition, which is the general case for oxides and nitrides. While, for instance by sputtering W or WS_2 in the presences of H_2S gas, it is possible to go from a sub-to-over-stoichiometric composition by increasing the H_2S flow. Therefore, it is a more complex material system.

Hysteresis measurements (increasing the reactive gas flow from zero (metal mode) to a flow far into the compound mode and back to zero, see section 2.5.1.) were performed for all material systems at different constant argon pressures ranging from 0.3 Pa to 2.7 Pa. By increasing the processing pressure a reduction of the hysteresis was observed, see *Figure 30*. However, a more pronounced reduction was observed for the low reactivity systems (Al in Ar/O_2 and Ti in Ar/N_2) where in fact the hysteresis was eliminated for a sufficiently high process pressure. These results were also confirmed by simulating these conditions.

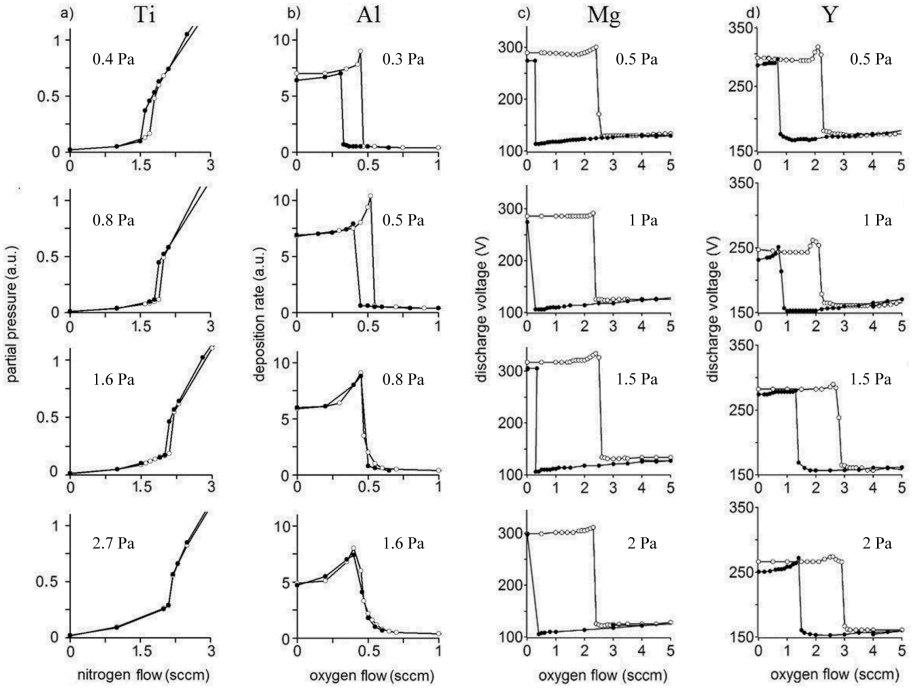

Figure 30. Process curves of different metal/reactive gas combinations sputtered at increasing total pressures. the reactive gas is stepwise increased (open circles) to a given maximum flow and the stepwise decreased (filled circles) to zero flow, (paper VI).

The simulations further showed that there was two effects present responsible for the poisoning of the target. At low pressures, both direct ion implantation and chemisorption are significant poisoning mechanisms, while the effect of direct ion implantation is removed at high pressures. Hence, only chemisorption is left making it possible to eliminate the hysteresis for low reactivity systems.

The well-known Berg model [31], which has proven to be an important tool in predicting the behaviour of reactive sputtering, does not account for different argon pressures or ion implantation effects. Therefore, it could not take different argon pressures into account in the simulations. Instead the reactive sputter deposition (RSD) model was used for the simulations in paper VI [69]. However, the RSD model is a rather complex several layer model not easily understood for the common engineer interested in reactive sputter processing. This is where the strength lays in the Berg model. Even though several effects have been disregarded, it still predicts the general trends of the system, making it possible to understand how a certain parameter affects the process. However, pressure dependency and ion implantation effects are clearly important for the reactive sputtering process. In paper VII, these new features are included (without complicating the mathematics) and

the upgraded model now accounts for atomic sputtering, direct ion and knock-in implantation and is pressure dependent (see paper VII for a detailed description or section 3.2. for a short version).

Hysteresis is a significant problem in reactive sputtering. There are, however, some methods to eliminate the hysteresis behaviour, see section 2.5.1. Kubart et al. has recently shown that by using sub-stoichiometric TiO_x targets ($x<2$) the hysteresis is eliminated for a certain sub-stoichiometric composition [26]. Our aim was to further investigate this for other materials and therefore we used a new approach based on the same idea by using segments of metal and its oxide. In paper VIII, this approach has been tested on Nb/Nb_2O_5, Ta/Ta_2O_5 and Al/Al_2O_3. It is here shown that the hysteresis is reduced and finally eliminated for increasing number of segments of oxide in the target. By eliminating the hysteresis, the unstable part is removed from the reactive sputtering process, making it possible to deposit stoichiometric coatings with an increased deposition rate. However, the gain won in deposition rate, compared with the deposition rate in compound mode, is dependent on the materials ability to form sub-oxides. In the case of Nb and Ta, the formation of sub-oxides decreases the maximum gain to an increase of 50% in deposition rate. For Al, on the other hand, which has no sub-oxides, the maximum gain in deposition rate is a factor of 10.

It is probably not practically applicable to use such segmented targets. In industrial applications, several metal targets are run simultaneously at high reactive gas flows to ensure stoichiometric film composition. This procedure involves a very low deposition rate. By replacing one or more metal targets with corresponding oxide target, a similar effect is achieved as demonstrated for segmented targets, which would result in the elimination of hysteresis and increased deposition rate and thus be of great interest.

7. Findings and outlook

The aim of this thesis is twofold; firstly, to obtain a fundamental understanding of the sputter deposition and the reactive sputter deposition processes through experiments and simulations, and secondly, to evaluate sputter deposition of specific materials system with low friction properties containing several elements and to improve their properties and add new features. This has been accomplished by studying the sputtering as well as the reactive sputtering process (papers IV-VIII) and by analysis, characterization and tribological testing of the deposited multi-elemental coatings (papers I-III).

The addition of titanium to the W-S-C system resulted in a new carbide phase TiC_xS_y, which significantly increased the hardness of the material (W-S-C-Ti) to 18 GPa (compared with 4 GPa for the corresponding W-S-C coating). In dry atmospheres, the friction was extremely high during the running-in phase. However, at steady-state conditions, the friction level was reduced but in general to a higher level than what was seen for the W-S-C system. However, the best W-S-C-Ti sample still showed the same low friction (μ =0.02) as the best W-S-C coatings. In humid environments, TiO_2 was formed in the wear tracks causing an increased friction. Therefore, no obvious improvements regarding the friction and wear in humid environments could be seen for the W-S-C-Ti system compared to the W-S-C system. However, the adhesion was slightly improved.

TMDs show excellent low friction properties in environments with low humidity or in vacuum. However, the challenge is to make them work properly and provide low friction even at humid conditions. Today the commercial use of TMDs (MoS_2 and WS_2) is almost exclusively as particle additives in fats and oils. The best existing commercial TMD coating is MoST (MoS_2 alloyed with Ti) which has shown improved resistance against oxidation [62]. However, it has a load bearing capacity of only 3 GPa. Therefore, the results found in paper I and II may be of great importance in the search of better mechanical properties in coatings able to perform in humid environments. The possibilities of reducing friction and wear in e.g. a pump or a car engine could result in massive energy and money savings, as well as, a much smaller environmental footprint, at a global scale.

The future lays in other/new material system. For instance, Gustavsson et al. recently published a paper on amorphous W-S-N coatings which demonstrated ultra-low friction ($\mu < 0.003$) against steel in a dry nitrogen atmosphere by the formation of WS_2 in the contact [70]. Other studies have shown

that diselenides have improved resistance to water in relation to sulphides [40, 71]. Further, improved performance has been observed for multilayer coatings of WS_2/MoS_2 at elevated temperatures [72]. Therefore, more research is needed in this area.

In paper III the new TiC_xS_y phase is further investigated. Here it is demonstrated that it is possible to incorporate as well as release sulphur from the coating. Ball-on-disc tests against a tungsten coated ball resulted in very low friction ($\mu = 0.05$) due to the formation of WS_2 in the wear track and on the ball. This opens up the possibilities of designing smart coatings. By adding elements with different purposes; some elements may form hard protective layers, while other elements can be activated by specific elements from the counter surface or atmosphere to form low friction in the contact.

Regarding sputtering of different elements, it is shown that if the mass of the sputtered atom is smaller or similar to that of the argon, a surprisingly large amount of the sputtered atoms will be backscattered and deposited in areas close to target even at low pressures (0.27 Pa). The opposite is true for much heavier atoms.

At high pressures (2.7 Pa), there are now so many collisions that all sputtered atoms are rapidly thermalized. Atoms, with a mass smaller or similar to argon, now have difficulties leaving the surroundings of the target and their propagation can more or less be described as a diffusion process. For the massive tantalum atom, a significant part is now being backscattered, but there is still some original directionality left.

When sputtering from a multi-element target, the different scattering behaviour of the different elements may cause significant pressure dependent compositional gradients over the chamber. This is qualitatively well known since long time but the results presented here now enable a quantitative estimation of such effect.

To get a deeper understanding of the sputtering process a Monte Carlo based program was developed following the target atoms from the ejection at the target surface through collisions in the gas phase and finally condensation at all the surfaces inside of the chamber. The simulations gave deposition profiles for the different elements and made it possible to predict the film stoichiometry. This was verified by experiments and proven correctly with adequate agreement.

Further, investigations of a more complex material system (WS_2) showed that the earlier explanation of sub-stoichiometry due to energetic particle bombardment causing re-sputtering of the growing film was insufficient. Here it is shown that one also must take scattering in the gas phase into account. In fact, the latter effect was demonstrated to be significantly larger than the previous one, making it possible to deposit $WS_{5.5}$ films. Other investigations is needed to find better optimization of the process parameters such as, target composition, target-to-substrate distance, better/smarter geometry of the chamber, other process gases (e.g. Ne, Xe), etc.

A commonly occurring effect in the reactive sputtering process is the hysteresis effect. It was noticed that the hysteresis behaviour was influenced by the total processing pressure. This was further investigated for four different reactive gas/material systems (Al, Mg, Y in Ar/O_2 and Ti in Ar/N_2). Both experiments and simulations showed that the hysteresis is reduced for increasing total processing pressures. However, the hysteresis was only eliminated for low reactivity systems (Al in Ar/O_2 and Ti in Ar/N_2), since at low pressures both direct ion implantation and chemisorption are significant poisoning mechanisms, while the effect of direct ion implantation is diminishing at high pressures. Hence, only chemisorption is left at high pressures making it possible to eliminate the hysteresis for low reactivity systems.

This new method of eliminating the hysteresis effect, lead to the upgrading of the Berg model, which in its original state is not dependent on the total processing pressure. The upgraded version now accounts for atomic sputtering, direct ion and knock-in implantation, and consequently a pressure dependency of the processing gas.

There are several ways of eliminating the hysteresis behaviour (see section 2.5.1.). Kubart et al. has recently shown that it is possible to eliminate the hysteresis by using sub-stoichiometric targets of TiO_x ($x<2$). The same idea is investigated for Nb/Nb_2O_5, Ta/Ta_2O_5 and Al/Al_2O_3, but the target now consists of segments of metal and its oxide instead of a homogeneously mixed target. Both experiments and simulations show that the hysteresis is reduced and eventually eliminated by increasing numbers of oxide segments in the target. However, the maximum gain in deposition rate depends on the materials ability to form sub-oxides with a high sputtering yield. Aluminium does not have any sub-oxides and it is therefore possible to deposit stoichiometric films with a 10 times higher deposition rate compared to the oxide target in compound mode. For niobium and tantalum, which both form sub-oxides wth relatively high sputtering yield, the maximum gain is only slightly above 50%. It is concluded that this method will eliminate the hysteresis for a certain composition of an arbitrary metal and its oxide.

8. Svensk sammanfattning

Dagens moderna samhälle kräver ständigt nytänkande samt förbättringar av befintliga processer för att kunna tillmötesgå kraven på bättre, snabbare, miljövänligare och billigare produkter. Detta gäller i synnerhet tunnfilmsindustrin vilket sätter stor press på dagens ingenjörer att finna nya material/materialkombinationer för att t. ex. kunna öka prestandan på en mobiltelefon genom större/snabbare minne, bättre skärmsupplösning, etc., samtidigt som den helst ska vara billigare än sin föregångare.

Tunnfilmsindustrin föddes för ungefär 160 år sedan och användes då främst för produktion av speglar och dekorativa beläggningar. När mikroelektronikindustrin senare tog fart för ungefär 40-50 år sedan, ledde detta till en snabb utveckling av olika processtekniker och nya användningsområden. Idag är tunnfilmer en del av vardagslivet med omfattande tillämpningar inom ett stort antal områden allt i från solceller och integrerade kretsar till skyddande nötningsbeständiga, eller endast rent dekorativa beläggningar.

En tunnfilm är ett väldigt tunt skickt (från några atomlager till några mikrometer tjockt) som beläggs på ytan av en komponent. Tunnfilmen kan bestå av ett eller flera material, som skiljer sig från komponenten (substratet) som bär tunnfilmen. Anledningen till att man belägger en tunnfilm är för att antingen tillföra egenskaper som substratmaterialet själv inte kan frammana eller så är tunnfilmen i sig själv själva produkten (t. ex. en solcell eller transistor). Tunnfilmen beläggs oftast i vakuum med hjälp av en speciell utrustning och extremt rena källmaterial. Det går därför att kontrollera mycket noggrant vilken tjocklek, struktur och materialsammansättning som tunnfilmen får, och därigenom även dess egenskaper, vilka är starkt beroende av tunnfilmens tjocklek, struktur och sammansättning. Det är därför möjligt att designa tunnfilmen så att den fungerar enligt specifika önskemål.

Det finns en uppsjö av olika metoder för att belägga en tunnfilm. I denna avhandling har tunnfilmerna belagts med hjälp av magnetronsputtring (katodförstoffning). I denna metod accelereras argonjoner av ett elektriskt fält mot en target (som består av det material som tunnfilmen ska byggas upp av). När argonjonerna kolliderar med targeten, slås atomer av targetmaterialet ut, vilka kommer att kondensera på komponenten (substratet) samt på resterande ytor i vakuumkammaren och bilda en tunnfilm (se *Figure 4* för en skiss över ett sputtringssystem). Genom att tillföra en reaktiv gas till processen (t. ex. syre eller kväve) är det möjligt att bygga upp en tunnfilm som har en annan sammansättning än targeten.

Syftet med denna avhandling är, för det första, att ge en ökad fundamental förståelse för hur sputtringsprocessen och den reaktiva sputtringsprocessen fungerar, och för det andra, att utvärdera specifika materialsystem med lågfriktionsegenskaper och förbättra deras egenskaper och prestanda. Detta har åstadkommits genom att studera och simulera sputtringsprocessen och den reaktiva sputtringsprocessen (papper IV-VIII) samt genom analys, karakterisering och tribologiska tester av de belagda tunnfilmerna (papper I-III).

WS_2 är känt för sin skicktade/lamellära struktur som ger upphov till dess mycket goda lågfriktionsegenskaper i vakuum eller luft med väldigt låg fuktighet. Tyvärr har WS_2 svaga mekaniska egenskaper vilket har begränsat dess användning som ytbeläggning.

I papper I och II, adderas även titan till W-S-C systemet. Detta resulterar i väsentligt hårdare beläggningar (18 GPa för W-S-C-Ti, att jämföra med 4 GPa för motsvarande W-S-C beläggning) på grund av skapandet av en ny karbidfas (TiC_xS_y). Den låga friktionen lyckas samtidigt bibehållas på grund av den starka drivkraften hos svavel och volfram att bilda en tribofilm av lättskjuvade WS_2 plan i nötningsspåret mellan ytorna. I papper III undersöks den nya TiC_xS_y fasen ytterligare genom simultan sputtring av titan och kol samtidigt som svavel tillförs reaktivt genom H_2S gas. Det visas här att de tillförda svavelatomer byter plats med kolatomerna i titankarbiden och att cellparametern därför växer. Vidare påvisas att det inlösta svavlet kan ”svettas” ut från bulken till ytan, vilket resulterar i att friktionen minskar något mot en stålkula för ökande svavelinnehåll i beläggningen. Dock vid användandet av en volframbelagd kula sågs en dramatisk sänkning av friktionen på grund av bildandet av WS_2 i glidkontakten.

I papper IV och V studeras olika utsputtrade grundämnens benägenhet att spridas vid kollisioner med argon i gasfasen. Vidare utvecklades ett Monte-Carlo baserat simuleringsprogram för att ge ytterligare förståelse om vilka effeketer som påverkar sputtringsprocessen. Programmet följer den utsputtrade atomen från att den sputtras ut från ytan på targeten genom kollisioner i gasfasen och slutligen kondensation på någon av ytorna inuti kammaren. Modellen verifierades först genom experiment av enklare system som bestod av två metaller i papper IV (i dessa system finns inga energetiska partiklar i form av negativa joner som kan återsputtra atomer från den växande filmen eller stora skillnander i sticking koefficienter) och applicerades därefter på ett mer komplicerat materialsystem (WS_2) i papper V. Här visade både experiment och simuleringar att den tidigare förklaringen till understökiometrisk sammansättning på filmer sputtrade från en WS_2 target inte var tillräcklig. Tidigare studier förklarade understökiometrin med energetiska partiklar som preferentiellt sputtrade svavel från den växande filmen medan våra resultat påvisade att sammansättningen även är starkt beroende av materialspecifika spridningseffekter genom kollisioner med argon. I själva verket visade sig den senare effekten vara betydligt mer framträdande och gjorde det möjligt

att belägga filmer från under- till över- stökiometrisk sammansättning beroende på substratets läge relativt targeten.

I papper VI-VIII studeras den reaktiva sputtringsprocessen vilken är väldigt komplex och oftast uppvisar ett hysteresbeteende. Detta innebär en instabilitet i processen som gör det tekniskt komplicerat att belägga en film inom ett visst processområde. Detta innebär normalt en kraftig sänkning av beläggningshastigheten.

I papper VI undersöks hur processtrycket påverkar hysteresen för fyra olika materialsystem (Al, Mg, Y i en Ar/O_2 atmosfär och Ti i en Ar/N_2 atmosfär) med varierande grad av reaktivitet. Både experiment och simuleringar visade att hysteresen minskade för ökande processtryck, men att hysteresen endast kunde elimineras för materialsystem med relativt låg reaktivitet (Al i en Ar/O_2 atmosfär och Ti i en Ar/N_2 atmosfär). Detta på grund av att två olika effekter kan ge upphov till att reaktiv gas bildar föreningar på targeten (förgiftning av targeten). Vid låga tryck är både direkt joninplantering och kemisorption significanta effekter, medan effekten av direkt joninplantering avtar vid högre processtryck.

Detta nya sätt att eliminera hysteresen, resulterade i en uppgradering av Berg-modellen (papper VII), vilken inte tar hänsyn till processtrycket av argongas i sin ursprungliga form. Den uppgraderade versionen inkluderar nu; atomär sputtring, direkt joninplantering, ”knock-in”-inplantering vilket indirekt ger ett beroende av processtrycket.

Det finns ytterligare sätt att eliminera hysteresbeteendet i reaktiv sputtring. I papper VIII undersöks en allternativ variant på en nyligen publicerad metod som visar att nyttjandet av en understökiometrisk homogent mixad oxidtarget kan användas för att minska och eliminera hystereseffekten. Vi applicerade denna metod på andra material och använde segment av metall och dess oxid istället för en homogent mixad target. Både experiment och simuleringar visade att hysteresen minskade och till sist elimineradesför ökat antal oxidsegment i targeten. I och med att hysteresen kan elimineras är det nu möjligt att belägga filmer vid tidigare tekniskt komplicerade processpunkter och dessutom med potentiellt betydligt högre beläggningshastighet.

Det är förmodligen inte praktiskt tillämpbart att nyttja dylika segmenterade targets. I industriella applikationer används flera metalltargets som körs samtidigt med höga reaktiva gasflöden för att säkerställa stökiometrisk filmsammansättning. Detta förfarande innebär en mycket låg beläggningshastighet. Genom att byta ut en eller flera metalltargets mot motsvarande oxidtarget skulle en liknande effekt uppnås som demonstrerats för segmenterade targets, vilket skulle resultera i eliminering av hysteresen och ökad beläggningshastigheten och därigenom vara av stort intresse.

Acknowledgements

Jag har haft några väldigt intressanta och utvecklande år i tunnfilmsgruppen. Ett stort tack till alla som bidragit till en arbetsmiljö som inte bara varit lärande utan även rolig, trevlig och uppmuntrande. Till och med i stunder då utrustning krånglat och gått sönder har det alltid funnits någon som hjälpt till, trots att dagen redan tagit slut. Ett särskilt tack skulle jag vilja rikta till

Tomas – som alltid tagit dig tiden att visa och förklara samt kommit med nya idéer och förslag. För alla diskussioner, jobbrelaterade eller ej, på jobbet eller någon annan stans i världen. Ett extra tack för alla otaliga timmar och dagar som du lagt ner på att hjälpa mig förbättra denna avhandling, trots att du haft semester.

Till alla kollegor i och runt Triboprojektet, speciellt Jill, Harald, Staffan, Ulf, Peter, Fredrik och Urban.

Till alla medförfattare i artiklar och konferencebidrag.

Tomas K – för att alltid hjälpt till vid stora som små problem i renrummet och för att alltid haft dörren öppen för att diskutera olika resultat.

Uwe – som alltid hjälpt mig då LEA och von Ardenne systemen råkat ut för nått problem fem över fem på kvällen.

Sören – för alla diskussioner, ideer och projekt under dessa år.

Marianne – som gång på gång hjälpt mig fylla i reseräkningar och betala konferenceavgifter på sista anmälningsdagen.

Shi-Li, Jörgen och Tobias – för er hjälp med korrekturläsningen av min avhandling.

Shabnam, Sara, Milena, Lina och Emil – för att ha lättat upp stämningen på kontoret genom roliga diskussioner och spratt men framför allt för att ha visat vägen till massagerummet.

Tove, Ray och Lotten – för att det gått så smidigt att planera och dela på von Ardenne systemet.

Bagge – för att ha räddat mig och denna avhandlig genom att få igång endnote som crashat två dagar *efter* inlämning.

Christopher – för dina försök att få mig att komma igång med träningen.

Patrik – för alla svar på frågor mellan himmel och jord.

Till alla övriga på FTE.

Till, sist men inte minst, min familj och alla vänner utanför forskarvärlden som stöttat och hjälpt, utan att aldrig riktigt veta vad jag sysslar med.

References

[1] M. Ohring, The Materials Sciencs of Thin Films, Academic Press, San Diego, 1992.

[2] J. Plücker, The London, Edinburgh, and Dublin Philosophical Magazine, 16 (1858).

[3] S.M. Rossnagel, Journal of Vacuum Science & Technology A, 21 (2003) S74-S87.

[4] J.L. Vossen, W. Kern, Thin Film Processes II, Academic Press, San Diego, 1991.

[5] Handbook of thin-film deposition processes and techniques, 2 ed., William Andrew Publishing/Noyes, 2002.

[6] P.M. Martin, Handbook of deposition technologies for films and coatings: science, applications and technology, 3rd ed ed., Elsevier, 2010.

[7] J. Musil, P. Baroch, J. Vlcek, K.H. Nam, J.G. Han, Thin Solid Films, 475 (2005) 208-218.

[8] S.M. D. Depla, Reactive sputter deposition, Springer-Verlag, 2008.

[9] Handbook of plasma processing technology, Noyes Publications, 1989.

[10] R. Behrisch, P. Sigmund, M.T. Robinson, H.H. Andersen, H.L. Bay, H.E. Roosendaal, Sputtering by Particle Bombardment I, Springer-Verlag, Berlin, 1981.

[11] J.F. Ziegler, J.P. Biersack, U. Littmark, in: J.F. Ziegler (Ed.) The Stopping and Range of Ions in Matter, Pergamon, New York, 1985.

[12] J.P. Biersack, L.G. Haggmark, Nucl Instrum Methods, 174 (1980) 257-269.

[13] W.R. Grove, Phil. Trans. Roy. Soc., London A, 142 (1852) 87.

[14] P. Carvalho, J.M. Chappe, L. Cunha, S. Lanceros-Mendez, P. Alpuim, F. Vaz, E. Alves, C. Rousselot, J.P. Espinos, A.R. Gonzalez-Elipe, J Appl Phys, 103 (2008).

[15] H. Sato, T. Minami, S. Takata, T. Yamada, Thin Solid Films, 236 (1993) 27-31.

[16] J.J. Chen, F. Zeng, D.M. Li, J.B. Niu, F. Pan, Thin Solid Films, 485 (2005) 257-261.

[17] W.D. Sproul, Thin Solid Films, 107 (1983) 141-147.

[18] A.C. Fernandes, F. Vaz, L. Cunha, N.M.G. Parreira, A. Cavaleiro, P. Goudeau, E. Le Bourhis, J.P. Riviere, D. Munteanu, B. Borcea, R. Cozma, Thin Solid Films, 515 (2007) 5424-5429.

[19] I. Safi, Surface and Coatings Technology, 127 (2000) 203-218.
[20] W.D. Sproul, Surface and Coatings Technology, 33 (1987) 73-81.
[21] T. Serikawa, A. Okamoto, Thin Solid Films, 101 (1983) 1-6.
[22] S. Kadlec, J. Musil, J. Vyskocil, Vacuum, 37 (1987) 729-738.
[23] T. Nyberg, S. Berg, U. Helmersson, K. Hartig, Appl Phys Lett, 86 (2005).
[24] D. Severin, O. Kappertz, T. Kubart, T. Nyberg, S. Berg, A. Pflug, M. Siemers, M. Wuttig, Appl Phys Lett, 88 (2006).
[25] D. Severin, O. Kappertz, T. Nyberg, S. Berg, A. Pflug, M. Wuttig, J Appl Phys, 105 (2009).
[26] T. Kubart, D. Depla, D.M. Martin, T. Nyberg, S. Berg, Appl Phys Lett, 92 (2008).
[27] J. Neidhardt, S. Mraz, J.M. Schneider, E. Strub, W. Bohne, B. Liedke, W. Moller, C. Mitter, J Appl Phys, 104 (2008).
[28] S. Berg, H.-O. Blom, T. Larsson, C. Nender, J. Vac. Sci Technol. A, 5 (1987) 202-207.
[29] S. Berg, T. Larsson, C. Nender, H.-O. Blom, J. Appl. Phys., 63 (1988) 887-891.
[30] H. Sekiguchi, A. Kanzawa, T. Imai, T. Honda, J. Vac. Sci. Technol. A, 12 (1994) 3176-3179.
[31] S. Berg, T. Nyberg, Thin Solid Films, 476 (2005) 215-230.
[32] F. Engelmark, G.F. Iriarte, I.V. Katardjiev, M. Ottosson, P. Muralt, S. Berg, J. Vac. Sci. Technol. A, Vac. Surf. Films, 19 (2001) 2664-2669.
[33] P. Lobl, M. Huppertz, D. Mergel, Thin Solid Films, 251 (1994) 72-79.
[34] J.A. Thornton, J Vac Sci Technol, 11 (1974) 666-670.
[35] I. Petrov, P.B. Barna, L. Hultman, J.E. Greene, J Vac Sci Technol A, 21 (2003) S117-S128.
[36] A. Anders, Thin Solid Films, 518 (2010) 4087-4090.
[37] J.A. Thornton, J Vac Sci Technol, 12 (1975) 830-835.
[38] A. Erdemir, C. Donnet, J Phys D Appl Phys, 39 (2006) R311-R327.
[39] T. Polcar, A. Cavaleiro, Thin Solid Films, 519 (2011) 4037-4044.
[40] T. Kubart, T. Polcar, L. Kopecky, R. Novak, D. Novakova, Surf Coat Tech, 193 (2005) 230-233.
[41] W.A. Brainard, The termal stability and friction of the disulfides, diselenides, and ditellurides of molybdenum and tungsten in vacuum (10-9 to 10-6 Torr), NASA scientific and technical publications, 1969.
[42] P.D. Fleischauer, Thin Solid Films, 154 (1987) 309-322.
[43] S.R. Cohen, L. Rapoport, E.A. Ponomarev, H. Cohen, T. Tsirlina, R. Tenne, C. Levy-Clement, Thin Solid Films, 324 (1998) 190-197.
[44] S. Fayeulle, P.D. Ehni, I.L. Singer, Surf Coat Tech, 41 (1990) 93-101.
[45] K.J. Wahl, I.L. Singer, Tribol Lett, 1 (1995) 59-66.

[46] C. Donnet, J.M. Martin, T. LeMogne, M. Belin, Tribol Int, 29 (1996) 123-128.
[47] J.K. Lancaster, Tribol Int, 23 (1990) 371-389.
[48] S.V. Prasad, J.S. Zabinski, N.T. Mcdevitt, Tribol T, 38 (1995) 57-62.
[49] P.D. Fleischauer, J.R. Lince, Tribol Int, 32 (1999) 627-636.
[50] V. Buck, Wear, 114 (1987) 263-274.
[51] T.W. Scharf, A. Rajendran, R. Banerjee, F. Sequeda, Thin Solid Films, 517 (2009) 5666-5675.
[52] B. Deepthi, H.C. Barshilia, K.S. Rajam, M.S. Konchady, D.M. Pai, J. Sankar, Surf Coat Tech, 205 (2010) 1937-1946.
[53] A. Nossa, A. Cavaleiro, Surf Coat Tech, 163 (2003) 552-560.
[54] A.A. Voevodin, J.P. O'Neill, J.S. Zabinski, Tribol Lett, 6 (1999) 75-78.
[55] T. Polcar, M. Evaristo, A. Cavaleiro, Plasma Process Polym, 4 (2007) S541-S546.
[56] A.A. Voevodin, J.S. Zabinski, Thin Solid Films, 370 (2000) 223-231.
[57] T. Polcar, M. Evaristo, A. Cavaleiro, Wear, 266 (2009) 388-392.
[58] T. Polcar, M. Evaristo, A. Cavaleiro, Vacuum, 81 (2007) 1439-1442.
[59] F. Gustavsson, P. Forsberg, V. Renman, S. Jacobson, Tribology - Materials, Surfaces & Interfaces, 6 (2012) 102-108.
[60] C. Muratore, A.A. Voevodin, Thin Solid Films, 517 (2009) 5605-5610.
[61] M. Regula, C. Ballif, M. Remskar, F. Levy, Journal of Vacuum Science & Technology a-Vacuum Surfaces and Films, 15 (1997) 2323-2329.
[62] K.J. Wahl, D.N. Dunn, I.L. Singer, Wear, 237 (2000) 1-11.
[63] K. Ellmer, Phys Status Solidi B, 245 (2008) 1745-1760.
[64] L.E. Rumaner, T. Tazawa, F.S. Ohuchi, Journal of Vacuum Science & Technology a-Vacuum Surfaces and Films, 12 (1994) 2451-2456.
[65] R.R. Olson, M.E. King, G.K. Wehner, J Appl Phys, 50 (1979) 3677-3683.
[66] D.B. Bergstrom, F. Tian, I. Petrov, J. Moser, J.E. Greene, Appl Phys Lett, 67 (1995) 3102-3104.
[67] S. Mahieu, G. Buyle, D. Depla, S. Heirwegh, P. Ghekiere, R. De Gryse, Nucl Instrum Meth B, 243 (2006) 313-319.
[68] T. Lemogne, C. Donnet, J.M. Martin, A. Tonck, N. Millardpinard, S. Fayeulle, N. Moncoffre, J Vac Sci Technol A, 12 (1994) 1998-2004.
[69] D. Depla, S. Heirwegh, S. Mahieu, R. De Gryse, J Phys D Appl Phys, 40 (2007) 1957-1965.
[70] F. Gustavsson, S. Jacobson, A. Cavaleiro, T. Polcar, Surf Coat Tech, 232 (2013) 541-548.
[71] A.R. Landsdown, Molybdenum disulphide lubrication, Elsevier, 1999.

[72] S. Watanabe, J. Noshiro, S. Miyake, Surf Coat Tech, 183 (2004) 347-351.

Acta Universitatis Upsaliensis

Digital Comprehensive Summaries of Uppsala Dissertations from the Faculty of Science and Technology 1162

Editor: The Dean of the Faculty of Science and Technology

A doctoral dissertation from the Faculty of Science and Technology, Uppsala University, is usually a summary of a number of papers. A few copies of the complete dissertation are kept at major Swedish research libraries, while the summary alone is distributed internationally through the series Digital Comprehensive Summaries of Uppsala Dissertations from the Faculty of Science and Technology. (Prior to January, 2005, the series was published under the title "Comprehensive Summaries of Uppsala Dissertations from the Faculty of Science and Technology".)

Distribution: publications.uu.se
urn:nbn:se:uu:diva-229207

ACTA
UNIVERSITATIS
UPSALIENSIS
UPPSALA
2014